AN INTEGRAL TURBULENT KINETIC ENERGY ANALYSIS OF FREE SHEAR FLOWS[1]

By C. E. Peters and W. J. Phares
ARO, Inc.

SUMMARY

Mixing of coaxial streams is analyzed by application of integral techniques. An integrated turbulent kinetic energy (TKE) equation is solved simultaneously with the integral equations for the mean flow. Normalized TKE profile shapes are obtained from incompressible jet and shear layer experiments and are assumed to be applicable to all free turbulent flows. The shear stress at the midpoint of the mixing zone is assumed to be directly proportional to the local TKE, and dissipation is treated with a generalization of the model developed for isotropic turbulence. Although the analysis was developed for ducted flows, constant-pressure flows were approximated with the duct much larger than the jet. The axisymmetric flows under consideration have been predicted with reasonable accuracy. Fairly good results have also been obtained for the fully developed two-dimensional shear layers, which were computed as thin layers at the boundary of a large circular jet.

INTRODUCTION

An extensive integral analysis of ducted turbulent mixing processes (fig. 1) has been developed at the Arnold Engineering Development Center (AEDC) (refs. 1 and 2). As usual with such analyses, the shape of the velocity profile is assumed, and the integral form of the mean flow governing equations is used to compute the shear-layer growth rate and other dependent variables of the problem. In the integral analysis of references 1 and 2, the turbulent shear stress at the midpoint of the shear layer is computed by use of a model for the turbulent eddy viscosity. The integral analysis has been extended to flows with equilibrium chemical reactions, to flows which extend across the entire mixing duct, and to flows in which the inviscid portion of the jet flow must be treated with the method of characteristics. The method has also been applied to flows with embedded recirculation zones. The analytical framework has been developed for

[1] The research reported in this paper was sponsored by the Arnold Engineering Development Center, Air Force Systems Command, Arnold Air Force Station, Tennessee, under Contract No. F40600-72-0003 with ARO, Inc. Major financial support was provided by the Air Force Office of Scientific Research, under Program Element 61102F, Project 9711. Dr. B. T. Wolfson was the project monitor.

quite complex flow situations, but a serious deficiency has always been the model used for the turbulent eddy viscosity, the Prandtl incompressible model with a compressibility correction similar to that proposed by Donaldson and Gray (ref. 3). This eddy-viscosity model is not adequate when the secondary stream velocity exceeds about 0.2 times the primary stream velocity, or when large pressure gradients exist in the flow field. Other eddy-viscosity models have been proposed which would perhaps yield better results for certain flows, but based on the extensive evaluation by Harsha (ref. 4), it is not likely that any eddy-viscosity model will be applicable to the entire range of free turbulent flows of interest. A fundamental problem with eddy-viscosity models is that the turbulent shear stress is related only to the local mean flow properties (this local dependence is true only in simple limiting flow situations); most free turbulent flows are characterized by significant history effects on the turbulent transport.

Starting with the work of Bradshaw and associates (ref. 5) a few years ago, considerable effort has been devoted to development of the turbulent kinetic energy (TKE) methods for turbulent shear flows. In these methods, the turbulent shear stress is related to the kinetic energy of the turbulent motion, and the TKE governing equation is solved simultaneously with the mean flow governing equations; the TKE equation is, in effect, a governing equation for the turbulent shear stress. Two different methods have been used to relate the shear stress to the TKE in free shear flows. In the work at AEDC (refs. 4, 6, and 7), Bradshaw's direct relationship between shear stress and TKE has been used. Other investigators (refs. 8 to 11) have related shear stress to TKE by defining an eddy viscosity which is the product of a length scale and the square root of the TKE. Although there appears to be experimental evidence (ref. 12) for the Bradshaw approach, both approaches are great improvements over earlier eddy-viscosity models in that turbulent shear flows are recognized to be indeed turbulent, that is, to consist of both mean and fluctuating components. The current TKE methods are undoubtedly oversimplified for the whole spectrum of turbulent flows in nature; however, Harsha's work (ref. 4) has shown that the TKE approach is useful for a large class of shear flows which is commonly encountered in engineering applications.

In the present study, the earlier integral approach for ducted flows (refs. 1 and 2) has been extended to include an integrated TKE equation. Because the TKE equation has been integrated across the entire shear layer, no model for the lateral diffusion of TKE needs to be specified. In addition, the relation between the TKE and the shear stress is specified only at the midpoint of the shear layer. These simplifications are achieved with a penalty – the shape of the lateral TKE profiles in the shear layer must be specified. The TKE profile shapes have been obtained from incompressible experiments but have been used with reasonable success for flows with large density gradients.

The present integral method is limited to those flows in which the velocity profile shape is essentially fully developed (shape similar) throughout the flow field; that is, the initial boundary layers must be relatively thin. Deference must be made to the more powerful finite-difference TKE methods for those flows which have developing velocity profiles over a significant axial distance. In addition, the present integral method has been formulated for only axisymmetric flow, and the two-dimensional jet and wake flows have not been computed. However, the fully developed shear layers (test cases 1 to 3) have been computed as thin layers at the boundary of a very large axisymmetric jet.

SYMBOLS

a_1	constant in TKE shear-stress relation
a_2	coefficient in dissipation term
b	mixing zone width
c	correction factor for a_2
C	mass fraction of elements from primary stream
D	diameter of primary stream nozzle
H	stagnation enthalpy
k	turbulent kinetic energy
$\bar{k}$	normalized turbulent kinetic energy
K	exponent in velocity-concentration relation
M	Mach number
M_e	external stream Mach number
M_o	central stream Mach number
n	boundary-layer profile exponent

p	static pressure
r	radial coordinate
r_i	radius of inner mixing zone boundary
r_o	radius of primary stream nozzle
r_w	duct wall radius
R	gas constant
R_T	turbulent Reynolds number
T	static temperature
T_t	stagnation temperature
u	axial velocity component
u_e	outer stream velocity
u_o	initial primary stream velocity
$\overline{u'^2}$	square of turbulent velocity component in x-direction
v	radial or transverse velocity
$\overline{v'^2}$	square of turbulent velocity component in r-direction
w	TKE profile parameter (eq. (11))
$\overline{w'^2}$	square of turbulent velocity component in circumferential direction
W	wake center-line velocity defect, $\frac{1 - u_c}{u_e}$
x	axial coordinate
x_{core}	length of first regime

y	transverse coordinate
$\bar{y}$	mixing zone coordinate, $\frac{r - r_i}{b}$
α	mass fraction of primary stream species on center line
δ	boundary-layer thickness
ϵ	turbulent eddy viscosity
ρ	density
τ	turbulent shear stress
σ	spreading parameter for two-dimensional shear layer
σ_o	spreading parameter at a reference condition

Subscripts:

1	initial mixing station; high speed stream for two-dimensional shear layer
2	low-speed stream for two-dimensional shear layer
a	inviscid secondary flow
bl	boundary layer
c	center line
f	far field
j	inviscid primary flow
m	half-velocity control surface in mixing zone
n	near field

sl	shear layer
w	duct wall

DEVELOPMENT OF ANALYSIS

The first and second regimes of figure 1 will be considered in this paper. A region of inviscid secondary flow exists throughout the duct, and the turbulent mixing zone is free turbulent in nature; that is, the turbulent flow is not adjacent to the wall. The duct wall interacts with the turbulent shear layer only through the axial-pressure gradients which are imposed by its presence.

Fundamental Assumptions

The following principal assumptions have been used in developing the analysis:

(1) The flow is axisymmetric.

(2) All gases obey the perfect gas law.

(3) The usual boundary-layer assumptions are used; that is, negligible radial pressure gradients, and so forth.

(4) The inviscid portions of the primary and secondary flows are one-dimensional and isentropic.

(5) The mixing layer is completely turbulent, and the initial boundary-layer thicknesses at the initiation of mixing are very small compared with the length of the first regime (fig. 1).

(6) The thickness of the nozzle lip separating the primary and secondary flows is negligible.

(7) The viscous effects at the duct wall are negligible.

(8) The normalized velocity profiles in the mixing layer are similar in shape at all axial stations and are represented by a cosine function.

(9) The turbulent Prandtl and Lewis numbers are unity.

(10) The TKE profile shapes in the shear layer which have been obtained from constant-density experiments are unaffected by density gradients in the shear layer.

(11) The turbulent kinetic energy outside the shear layer boundaries is negligible.

Basic Integral Equations

Nomenclature for the analysis is illustrated in figure 1. In this section, the nomenclature is generally consistent with that of references 1 and 2; the results are described in terms of the recommended nomenclature for this conference.

By integrating the boundary-layer differential equations, five basic integral equations are obtained: (1) a continuity equation for the entire flow, (2) a momentum equation for the entire flow, (3) a momentum equation for the flow between the duct center line and a control surface arbitrarily located at the midpoint of the shear layer, (4) a jet species conservation equation for the entire flow, and (5) a turbulent kinetic energy equation for the shear layer.

Continuity equation:

$$\int_0^{r_w} \frac{\partial}{\partial x}(\rho u) r \, dr = -\rho_w v_w r_w = -\rho_a u_a r_w \frac{dr_w}{dx} \tag{1}$$

Overall momentum equation:

$$\int_0^{r_w} \frac{\partial}{\partial x}(\rho u^2) r \, dr = -\frac{r_w^2}{2}\frac{dp_w}{dx} - \rho_a u_a^2 r_w \frac{dr_w}{dx} \tag{2}$$

Half-radius momentum equation:

$$\int_0^{r_m} \frac{\partial}{\partial x}(\rho u^2) r \, dr - u_m \int_0^{r_m} \frac{\partial}{\partial x}(\rho u) r \, dr = \tau_m r_m - \frac{r_m^2}{2}\frac{dp_w}{dx} \tag{3}$$

Jet species conservation equation:

$$\int_0^{r_w} \frac{\partial}{\partial x}(\rho u C) r \, dr = 0 \tag{4}$$

The differential form of the TKE equation is

$$\rho u r \frac{\partial k}{\partial x} + \rho v r \frac{\partial k}{\partial r} = \tau r \frac{\partial u}{\partial r} + \text{Diffusion} - \text{Dissipation}$$

where

$$k = \frac{1}{2}\left(\overline{u'^2} + \overline{v'^2} + \overline{w'^2}\right)$$

By integrating the TKE equation across the entire shear layer, the lateral diffusion term disappears. The dissipation is given by the usual relation developed for isotropic turbulence (ref. 4):

$$\text{Dissipation} = \frac{a_2 \rho k^{3/2} r}{b}$$

Thus, the basic integral TKE equation is

$$\int_{r_i}^{r_i+b} \frac{\partial}{\partial x}(\rho u k) r \, dr = \int_{r_i}^{r_i+b} \tau \frac{\partial u}{\partial r} r \, dr - \frac{a_2}{b} \int_{r_i}^{r_i+b} \rho k^{3/2} r \, dr \tag{5}$$

Velocity Profile

The velocity profile is given by

$$\frac{u - u_a}{u_c - u_a} = \frac{1}{2} + \frac{1}{2} \cos(\pi \bar{y}) \tag{6}$$

where $\bar{y} = \frac{r - r_i}{b}$ and $u_c = u_j$ in the first regime. The cosine profile is shown in figure 2, along with the experimental results of Spencer (ref. 13) for a fully developed two-dimensional shear layer. At the control surface, $r_m \left(= r_i + \frac{b}{2}\right)$, the velocity is

$$u_m = \frac{1}{2}(u_c + u_a)$$

Concentration and Enthalpy Profiles

For unity Lewis number, the normalized total enthalpy and concentration profiles are essentially identical and are related to the velocity profile by

$$C = \frac{H - H_a}{H_j - H_a} = \left(\frac{u - u_a}{u_j - u_a}\right)^K \tag{7}$$

The parameter K has been introduced so that jet species can be conserved in variable pressure flows. For unity turbulent Prandtl number, equation (7) with $K = 1$ is identically true for constant-pressure flow; the pressure gradients in all the flows considered in this communication are negligible, and K remained unity for all computations. Therefore, equation (4) could have been deleted for these flows, since the assumption of $K = 1$ would have identically satisfied that equation.

Turbulent Kinetic Energy Profiles

As with the velocity profile, the shape of the TKE profiles must be specified. The near-field (first-regime) TKE profiles have been obtained from the experimental results of Spencer (ref. 13) and Liepmann and Laufer (ref. 14) for constant-density two-dimensional shear layers. The experimental results are shown in figure 3, along with the following analytical function which has been fitted to the data:

$$\bar{k}_n = \frac{k}{k_m} = 0.51 - 0.51 \cos \frac{\pi \bar{y}}{0.45} \qquad (0 \leq \bar{y} \leq 0.45) \tag{8a}$$

$$\bar{k}_n = 0.51 - 0.51 \cos\left[2\pi(0.0909 + 0.9091\bar{y})\right] \qquad (0.45 \leq \bar{y} \leq 1.0) \qquad (8b)$$

In fitting the data, the recent experiments of Spencer were given more weight than the Liepmann and Laufer experiments because of the improvement of hot-wire techniques in the past 20 years.

In the far field, well downstream of the end of the potential core, the experiments of Pindell (ref. 15) and Wygnanski and Fiedler (ref. 16) on the constant-density axisymmetric jet into still air were used. The experimental TKE profiles are shown in figure 4, along with the following analytical function which has been fitted to the data:

$$\bar{k}_f = 0.5 + \sin\frac{\pi}{2}\left(1 + \frac{4}{3}\bar{y}\right) \qquad (9)$$

Obviously, the shape of the TKE profile cannot change discontinuously from $\bar{k}_n$ to $\bar{k}_f$ at the end of the first regime. It has been hypothesized that a transition region exists in which the TKE profile evolves from $\bar{k}_n$ to $\bar{k}_f$. In this transition region, the TKE profile is assumed to be a linear combination of $\bar{k}_n$ and $\bar{k}_f$

$$\bar{k} = w\bar{k}_f + (1 - w)\bar{k}_n \qquad (10)$$

where w is an empirical function of x. The resulting family of TKE profiles is shown in figure 5. Because many features of jets scale with x/x_{core}, it has been hypothesized that w can also be related to x/x_{core}. The experiments of Pindell (ref. 15), Sami (refs. 17 and 18), and Bradshaw et al. (ref. 19) on the constant-density jet were used to develop the following empirical function for w:

$$w = 1 - \exp\left[-1.09\left(\frac{x}{x_{core}} - 1\right)\right] \qquad (11)$$

The center-line TKE, normalized with the value at r_m, is shown in figure 6 for the constant-density jet into still air. A value of $x_{core} = 4.66D$ was used in computing the curve shown in figure 6; this core length is predicted by the present theory for a jet with negligible initial boundary layer. The TKE profiles are seen to be essentially fully developed ($w \approx 1$) for x greater than $5x_{core}$. It should be noted that the value of x_{core} is not prescribed for a particular flow but is a result of the first-regime solution.

Even though the TKE profile shapes were obtained from relatively simple constant-density flows, the two-dimensional shear layer and the axisymmetric jet, it is assumed that these profile relationships apply to all flows. It should be noted that nothing has been stated about the level of TKE, but only that the TKE profiles, normalized with k_m, are given by equations (8) to (11).

Relation Between TKE and Shear Stress

As the present integral theory has been formulated, the relationship between τ and k must be specified only at the midpoint of the shear layer r_m. This method is

distinctly different from finite-difference TKE methods, in which it is necessary to specify the variation of τ with k across the entire mixing zone. The linear relationship

$$|\tau_m| = a_1 \rho_m k_m \tag{12}$$

is used, with $a_1 = 0.3$, the value found by Harsha and Lee (ref. 11) in the high shear region of a variety of constant-density free turbulent flows. This value of a_1 is also the same as that used by Bradshaw et al. (ref. 5) for turbulent boundary layers. In order to have the proper sign on τ_m, equation (12) is written as

$$\tau_m = \frac{a_1 \rho_m k_m (u_a - u_c)}{|u_a - u_c|} \tag{13}$$

The Dissipation Parameter a_2

In the extensive evaluation of his differential TKE method (ref. 4), Harsha used $a_2 = 1.5$. During the development of the present integral method, $a_2 = 1.69$ was found to give good results for constant-density two-dimensional shear layers and for the axisymmetric jet into still air. Other flows, however, were found to require significantly different values for a_2 if reasonably good mean flow predictions were to be achieved. Specifically, supersonic flows require a_2 to be larger than 1.69, and some flows with very high shear stress levels require a_2 to be less than 1.69. Finally, it was found that a_2 could be correlated with the turbulent Reynolds number R_T which is defined as

$$R_T = \frac{|u_c - u_a| b}{\epsilon_m}$$

where ϵ_m is the local eddy viscosity at r_m. Of course, the eddy viscosity is not specified but is computed from

$$\epsilon_m = \frac{\tau_m}{\rho_m \left.\frac{\partial u}{\partial r}\right|_m}$$

For the cosine profile,

$$\left.\frac{\partial u}{\partial r}\right|_m = \frac{\pi (u_a - u_c)}{2b}$$

and R_T may be written as

$$R_T = \frac{\pi (u_c - u_a)^2}{2 a_1 k_m} = 5.236 \frac{(u_c - u_a)^2}{k_m}$$

Thus, it has been found that the dissipation coefficient a_2 can be related to the ratio of the mean flow velocity difference across the shear layer to the turbulent velocity fluctua-

tion level (characterized by k_m) in the layer. The a_2 function which has been developed is shown in figure 7, along with the equations which describe the function.

The approach used in the development of the $a_2 - R_T$ function will be briefly described. For $R_T > 145$, the a_2 function was developed by computational experiments on the near field of unheated compressible air jets exhausting into still air. Warren's potential core length data (ref. 20) for experimental flows with thin initial boundary layers and $0.69 < M_j < 2.6$ were used to establish approximately a few desired a_2 values. A direct correlation of a_2 with a characteristic Mach number for the shear layer was abandoned because such a correlation fails for two-stream supersonic flows such as the combustion flows reported in reference 1. The turbulent Reynolds number was finally found to correlate consistently the a_2 values for the preceding flows. Because R_T is related to the local turbulence characteristics in the shear layer, it is more appropriate as a dissipation parameter than some other parameter which is related only to the mean flow in the layer. When it is considered that only the near-field results for a few experimental flows were used in developing the a_2 function for $R_T > 145$, the overall performance of this part of the $a_2 - R_T$ function (fig. 7) has been reasonably satisfactory for a variety of flows. The high R_T portion of the a_2 function is subject to further refinement, however, particularly for $R_T > 300$, that is, for fully developed single stream flows with $M_j > 2.7$.

Experience with far-field predictions of jets in moving streams indicated that a_2 should be somewhat less than 1.69 for $R_T < 70$. The function used for $R_T < 70$ (fig. 7) is the first one tried, and no attempt has been made to improve it.

The effects of density ratio caused by jet Mach number are adequately predicted by the $a_2 - R_T$ function; however, prediction of the entire range of flows of interest is improved if small additional corrections to a_2 are made as a function of density ratio. Tentatively, the following corrections have been developed and used:

$$a_2 = \frac{a_2(R_T)}{c}$$

where $a_2(R_T)$ is as shown in figure 7 and c is given by

$$c = 0.984 + 0.016 \frac{\rho_{a1}}{\rho_{j1}} \qquad (\rho_{a1} > \rho_{j1})$$

or

$$c = 0.95 + 0.05 \frac{R_a T_{ta}}{R_j T_{tj}} \qquad (\rho_{a1} < \rho_{j1})$$

These density corrections to the basic $a_2 - R_T$ function are perhaps required because the empirical TKE profiles are inadequate for flows with large density gradients; this

point will not be resolved until detailed turbulence structure data are available for flows with large density gradients.

The a_2 function as described has been used for all of the shear layer and jet computations presented in this paper. Experience has shown that wakes require somewhat different dissipation than jet flows, and the axisymmetric wake computations (test cases 15 and 17) were made with $a_2 = 1.40$.

Turbulence Production

The first term on the right-hand side of equation (5) represents the production of turbulence by the shear stress. For the boundary conditions of the shear layer, the production is equal but opposite in sign to the dissipation of mean flow mechanical energy:

$$\int_{r_i}^{r_i+b} \tau \frac{\partial u}{\partial r} r \, dr = -\int_{r_i}^{r_i+b} u \frac{\partial}{\partial r}(\tau r) \, dr = -\frac{1}{2}\int_0^{r_i+b} \frac{\partial}{\partial x}(\rho u^3) r \, dr$$

$$+ \frac{1}{2} u_a^2 \int_0^{r_i+b} \frac{\partial}{\partial x}(\rho u) r \, dr - \frac{dp_w}{dx}\int_0^{r_i+b} ur \, dr \qquad (14)$$

By substituting equation (14) into equation (5), the following form of the integral TKE equation is obtained:

$$\int_{r_i}^{r_i+b} \frac{\partial}{\partial x}(\rho u k) r \, dr = -\frac{1}{2}\int_0^{r_i+b} \frac{\partial}{\partial x}(\rho u^3) r \, dr + \frac{1}{2} u_a^2 \int_0^{r_i+b} \frac{\partial}{\partial x}(\rho u) r \, dr$$

$$- \frac{dp_w}{dx}\int_0^{r_i+b} ur \, dr - \frac{a_2}{b}\int_{r_i}^{r_i+b} \rho k^{3/2} r \, dr$$

By using the TKE equation in this form, the shape of the shear-stress profile need not be specified. The turbulence production is related only to the dissipation of mean flow mechanical energy, which, in turn, is related to the mean flow profiles and the rate of growth of the shear layer.

Solution Technique

Sufficient information is available to transform equations (1) to (5) into a system of ordinary differential equations which is linear in the derivatives of the dependent variables $(dp_w/dx$, etc.$)$. This transformation procedure is described in detail in reference 2. After the system of linear equations is solved for the derivatives, the resulting five differential equations are then numerically integrated with a modified Euler technique (variable step size). An IBM 370/155 digital computer was used to obtain the numerical solutions; a typical flow-field solution required a computation time of approximately 2 minutes.

In the first regime, the dependent variables are p_w, r_i, b, K, and k_m. In the second regime, the dependent variables are p_w, u_c, b, K, and k_m.

Initial Conditions

In order to integrate the system of differential equations, initial values must be specified for each of the dependent variables. The most critical of these initial values is that for k_m. As usual with TKE methods, the convective terms cause the initial condition for k_m (or τ_m) to be "remembered" for some distance downstream; the distance is dependent on the particular flow situation. Experience has shown that two stream flows with $u_a/u_j < 0.25$ can be started with a "fully developed" shear stress. This fully developed shear stress is obtained from the corresponding fully developed two-dimensional shear layer. Even though the present method is generally limited to flows with thin initial boundary layers, two stream jet flows with $u_a/u_j < 0.25$ and very thick initial boundary layers (jet nozzle boundary-layer thickness up to $0.4r_o$) have been successfully computed with the following procedure: (1) the initial boundary layer is assumed to be negligible, and (2) the inner shear layer radius r_i is adjusted to match the experimental value of the excess momentum.

Even for thin boundary layers, the influence of the initial conditions persists throughout the flow field when u_a/u_j exceeds about 0.3. Therefore, the concept of a negligible initial boundary layer and a fully developed initial shear stress is not usable for such flows. In order to treat these flows, a control volume analysis of the initial region has been developed.

Control Volume Analysis of Initial Region

A sketch of the initial region just downstream of the nozzle lip is shown in figure 8. The initial boundary layers are characterized by power law velocity profiles:

$$\frac{u}{u_a} = \left(\frac{r - r_o}{\delta_a}\right)^{n_a}$$

and

$$\frac{u}{u_j} = \left(\frac{r_o - r}{\delta_j}\right)^{n_j}$$

The nozzle wall is assumed to be adiabatic; therefore, the stagnation temperature is constant in each boundary layer. Specification of the wall skin-friction coefficients, c_{fa} and c_{fj}, and $a_1 = 0.3$ completely defines the mean flow and the turbulence quantities at the initial station $b\ell$. The wall skin-friction coefficients are determined with the method of Spalding and Chi (ref. 21).

At some downstream station, $s\ell$, the flow is assumed to have evolved to the fully developed shear layer profile shapes for velocity and near-field TKE. The following assumptions are made about the process between $b\ell$ and $s\ell$:

(1) There is no net entrainment into the shear layer.

(2) The process occurs at constant pressure.

(3) The excess momentum is conserved.

(4) The length scale of the process is sufficiently small to insure that the volume integral of turbulent dissipation is negligible.

The following equations are written between stations $b\ell$ and $s\ell$:

Momentum:

$$\int_0^{r_o+\delta_a} \rho u(u - u_a) r \, dr \Big|_{b\ell} = \int_0^{r_i+b} \rho u(u - u_a) r \, dr \Big|_{s\ell} \tag{15}$$

Continuity:

$$\int_{r_o-\delta_j}^{r_o+\delta_a} \rho u r \, dr \Big|_{b\ell} = \int_{r_i}^{r_i+b} \rho u r \, dr \Big|_{s\ell} \tag{16}$$

Turbulent kinetic energy:

$$\int_{r_o-\delta_j}^{r_o+\delta_a} \rho u k r \, dr \Big|_{b\ell} + \frac{1}{2} \int_{r_o-\delta_j}^{r_o+\delta_a} \rho u^3 r \, dr \Big|_{b\ell} + \frac{1}{4} \rho_j u_j \left(u_j^2 - u_a^2\right) \left[\left(r_o - \delta_j\right)^2 - r_i^2\right]$$

$$= \int_{r_i}^{r_i+b} \rho u k r \, dr \Big|_{s\ell} + \frac{1}{2} \int_{r_i}^{r_i+b} \rho u^3 r \, dr \Big|_{s\ell} \tag{17}$$

With δ_a, δ_j, n_a, n_j, c_{fa}, and c_{fj} specified, equations (15) to (17) are solved for r_i, b, and k_m. These values are then used as initial conditions for the integral TKE solution of the remainder of the flow field.

This control volume analysis is obviously not applicable as u_a/u_j approaches unity, since in such flows a very large distance is required to approach a fully developed profile shape. In addition, the initial region analysis as formulated is not applicable to mixing of streams with greatly different densities. The computations are made with $K = 1$ at station $s\ell$, and the solution does not, in general, conserve species or energy.

RESULTS AND DISCUSSION

Initial conditions for the computed experimental flows are presented in table I. The initial shear stress levels are characterized by the turbulent Reynolds number R_T. In addition to being used to specify the initial shear stress, the axial distribution of R_T throughout the flow field is very informative, and a number of such distributions is presented. For the cosine profile, the midpoint shear stress in the mixing layer is given by

$$\frac{|\tau_m|}{\rho_m(\Delta u)^2} = \frac{\pi}{2R_T}$$

where Δu is the local velocity difference across the layer. If self preservation is approached, then R_T must become constant in the flow field.

Most of the flows considered in this conference have a constant-pressure boundary condition, whereas the analysis was developed for a ducted system with a prescribed duct wall shape. The constant-pressure axisymmetric flows were computed in a very large cylindrical duct ($r_w = 1000r_o$) so that negligible axial pressure gradients were predicted. Integrated momentum in the duct is conserved to a high degree of accuracy in the computations, typically to within one part in 10^5. The degree to which the jet excess momentum is conserved in constant-pressure flows is illustrated by the fully developed axisymmetric jet (test case 18). For similar velocity profiles, the product of mixing zone width and center-line velocity should remain constant throughout the second regime. This product changed 1.5 percent from the value at the end of the core at $x/D = 50$, and 2.8 percent at $x/D = 100$. Even though the excess jet momentum is not exactly conserved in the calculations because of the ducted boundary condition, the results are considered to conserve excess momentum adequately when the inprecision of most experiments is taken into account.

Effect of Velocity Ratio on Growth of Fully Developed Two-Dimensional Shear Layer – Test Case 1

As presently formulated, the integral analysis cannot be used for zero secondary velocity. Therefore, all computations of flows with nominal zero secondary velocity were made with a secondary velocity 0.01 times the maximum velocity in the flow field (u_1 or u_o). The fully developed two-dimensional shear layers were computed as thin shear layers at the boundary of a large axisymmetric jet; the duct radius r_w was set equal to $100r_o$ for these cases. In no case did the predicted shear-layer thickness exceed 2 percent of the jet radius.

Computations for test case 1 were made for $u_2/u_1 = 0.01$, 0.2, 0.4, 0.6, and 0.8. The results, shown in figure 9 (test case 1), fall on the classic relationship

$$\frac{\sigma_o}{\sigma} = \frac{u_1 - u_2}{u_1 + u_2}$$

where $\sigma_o = 12.9$ for $u_2/u_1 = 0$. The standard relation for σ used in this computation becomes

$$\sigma = \frac{3.12}{db/dx}$$

for the cosine profile. It should be noted that $\sigma = 12.9$ by this definition corresponds to $\sigma = 12$ when the cosine profile midpoint slope is matched to the widely used error function profile. The fully developed R_T varied negligibly from 143 over the entire range of u_2/u_1.

Effect of Mach Number on Growth of Fully Developed Two-Dimensional Shear Layer – Test Case 2

Results for test case 2 are shown in figure 10(a). The computations were made with $u_2/u_1 = 0.01$; therefore, all σ values are about 2 percent too large. The ratio σ_o/σ, where σ_o is the value at $M_1 = 0$, is shown in figure 10(b), along with the value of fully developed R_T. Based on available experimental information on σ, the predicted σ_o/σ probably decreases too abruptly in the M_1 range of 0.5 to 1.5. The predicted σ values in this M_1 range can be altered by slight refinements of the a_2 function in the appropriate R_T range. The predicted σ values are considered to be good at $M_1 = 2$ and $M_1 = 3$.

Effect of Density Ratio on Growth of Fully Developed Two-Dimensional Shear Layer – Test Case 3

The computations for test case 3 were made for low-speed flow and $u_2/u_1 = 0.2$. Results for σ and R_T are shown in figure 11 as a function of ρ_1/ρ_2. Evaluation of the σ predictions at high ρ_1/ρ_2 is nearly impossible because of the lack of experiments in this range. The σ results for this case are not influenced by the factor which causes the density ratio, that is, temperature difference or molecular weight difference.

In general, very large axial distances were required to approach the fully developed condition in all these shear-layer computations. All the flows were computed for an axial distance of several hundred initial shear-layer thicknesses; such distances were required to approach closely the fully developed condition unless the initial shear stress was luckily chosen to be very close to the fully developed value. These results clarify the extreme difficulty in accomplishing a shear-layer experiment in which the flow truly approaches a fully developed condition.

Maestrello and McDaid Axisymmetric Jet – Test Case 6

The computations for test case 6 were made in two ways. In the first (curve a, fig. 12), the experimental profile at $x/r_o = 2$ was fitted with a cosine profile, and the computations were started with a fully developed shear stress. The predicted rate of mixing is too large; therefore, the shear stress does not yet approach the fully developed value at $x/r_o = 2$ but is somewhat lower. The computations were also started at $x = 0$, with negligible initial boundary layer, fully developed R_T and r_i corrected to achieve the excess momentum shown at $x = 2r_o$. This second computation (curve b, fig. 12) yields a first regime which is somewhat too long, but the results are better than those of the first computation.

The abrupt change in center-line velocity at the end of the first regime is characteristic of the integral method but is of little concern unless the main interest is in the transition region at the end of the potential core.

Eggers Supersonic Jet Into Still Air – Test Case 7

The prediction of this well-defined experimental flow (test case 7) is very satisfactory. (See fig. 13(a).) Computations were started by assuming a negligible initial boundary layer and fully developed R_T (from fig. 10(b)). The predicted potential core is slightly longer than that shown by the experiment, but the far-field agreement is excellent. The predicted velocity profiles at $x/r_o = 8$, 27, and 99 are also satisfactory. (See fig. 13(b).) These profiles illustrate that the cosine profile approaches zero at the outer edge of the layer more rapidly than does the experiment; the cosine profile is generally better for two stream flows.

The predicted axial variation of R_T (fig. 13(c)) shows a very large change in R_T for this flow (from 283 to 82). Thus, most of the $a_2 - R_T$ function (fig. 7) was used in this prediction.

G.E. Heated Subsonic Jet – Test Case 8

The experimental velocity profile at $x/D = 2.79$ was fitted with a cosine profile; the computations were started with this velocity profile and fully developed R_T. Predictions of both center-line velocity and center-line static temperature are very satisfactory for test case 8. (See fig. 14.)

Forstall Jet in Moving Stream – Test Case 9

This flow (test case 9) was computed by assuming a thin initial boundary layer and fully developed R_T; r_i was corrected to yield the experimental excess momentum and the actual duct radius $r_w/r_o = 16$ was used for the prediction. The predicted center-

line velocity agrees very well with the experiment at all axial locations. (See fig. 15(a).) The detailed far-field behavior of the excess center-line velocity is illustrated in the log plot (fig. 15(b)). Because of the assumption of unity Prandtl and Lewis numbers, the predicted α is identical to the excess velocity $(u_c - u_e)/(u_o - u_e)$. Predicted half-velocity width (fig. 15(c)) agrees well with the experiment for x/D up to 25, but falls about 10 percent under the experiment at $x/D = 80$.

Chriss Hydrogen Jet in Moving Air Stream – Test Case 10

This flow (test case 10) was computed in two ways. In the first, a cosine velocity profile was fitted to the data at $x/D = 2.97$. This profile, along with the experimental shear stress shown in reference 22 $(R_T = 98.3)$, was used to start the computations. Predicted results for the center-line velocity are fairly good (fig. 16(a)), but the predicted rate of decay of center-line concentration is too low. This type of concentration prediction is typical of the integral analysis, since it is limited to unity turbulent Prandtl and Lewis numbers.

The second computation was started at $x = 0$ with small initial shear layer thickness and fully developed shear stress $(R_T = 120)$. Predicted center-line velocities (fig. 16(b)) are somewhat better than those for the first computation, but, of course, the center-line concentration decay rate is again underpredicted.

Eggers and Torrence Axisymmetric Jet in Moving Air Stream – Test Case 11

This flow (test case 11) has wakelike behavior and it is unlikely that it can be properly predicted by a constant-pressure mixing analysis. In spite of the thick initial boundary layers and the velocity ratio $(u_e/u_j = 1.36)$, computations were started at $x = 0$ with thin initial shear layer and fully developed shear stress. The predicted center-line velocity distribution is surprisingly close to the experiment. (See fig. 17.) Wakelike jet flows, with jet momentum flux less than external stream momentum flux, tend to have relatively high relative shear levels (low R_T), and it is possible in such flows that the influence of the initial conditions does not persist very far downstream in the flow field. This aspect should certainly be further explored.

Eggers Hydrogen Jet in Moving Air Stream – Test Case 12

As with the preceding case, this flow (test case 12) has jet momentum flux less than external stream momentum flux. In this case, however, the jet momentum deficit is caused by density rather than by velocity $(u_e/u_j = 0.37)$. Again, the computations were started with a thin initial shear layer and fully developed R_T. Although the length of the

first regime is somewhat overpredicted (fig. 18), the downstream prediction for both center-line velocity and center-line concentration is very good. In view of the unity Schmidt number assumption, the good prediction of both velocity and concentration was unexpected; the results are undoubtedly caused in part by the neglect of the initial boundary layers.

Chevray Axisymmetric Wake – Test Case 15

Computation of this flow (test case 15) was started at $x = 0$ with an equivalent second regime cosine velocity profile; the cosine profile was selected to match the experimental momentum defect and mass flow in the shear layer. An initial value for R_T was established by equating the experimental TKE flux (ref. 23) with the TKE flux in the equivalent fully developed profile. The theory does not predict the initial rapid acceleration of the center-line velocity (fig. 19(a)) for $x/D < 2$. This rapid acceleration is caused in part by a favorable pressure gradient just downstream of the body; the axial pressure gradient was neglected in the calculations. For $x/D > 4$, the center-line velocity defect W is underpredicted; however, the log plot of W against x (fig. 19(b)) shows that the predicted decay rate at $x/D = 18$ is somewhat less than the experimental rate. The predicted axial distribution of W follows an x^{-1} decay from $x/D = 5$ to the maximum axial distance computed ($x/D = 200$). Better prediction of the decay rate at $x/D = 18$ would require less dissipation than that used in the calculations. On the other hand, achievement of the $x^{-2/3}$ decay rate for W, as predicted for self-preservation, would require much higher dissipation. One can only conclude that (1) the far-field dissipative mechanism is much different from the near-field mechanism, or (2) self-preserving axisymmetric wakes are never attained. The lack of far-field experiments on the axisymmetric wake makes it difficult to decide which of these conclusions is correct.

The predicted axial variation of R_T (fig. 19(c)) shows that R_T never approaches a constant value but continuously decreases in the axial direction.

Demetriades Supersonic Axisymmetric Wake – Test Case 17

This flow (test case 17) was computed by fitting a cosine profile to the experimental velocity data at $x/D = 17$, and by using the R_T value quoted by Demetriades (ref. 24) for $x/D = 17$. The plot of $\frac{1}{W^{3/2}}$ against x/D (fig. 20(a)) shows that the experimental center-line velocity defect is well predicted. A log plot (fig. 20(b)) shows that the predicted W decays even more rapidly than an x^{-1} decay. Again, this axisymmetric wake prediction is very different from the $x^{-2/3}$ decay of W which is required for self-preservation. The predicted axial variation of R_T (fig. 20(c)) is considerably different from that shown by Demetriades (ref. 24); he showed R_T to be nearly constant at 32 for x/D greater than about 30.

Fully Developed Axisymmetric Jet – Test Case 18

This important and fundamental flow (test case 18) was computed from $x = 0$ by assuming a thin initial shear layer and a fully developed near-field shear stress $(R_T = 143)$. The predicted center-line velocity (fig. 21(a)) follows an x^{-1} decay for x/D greater than 15. Although the predicted center-line velocity agrees well with the experiment of Albertson et al. (ref. 25) at all axial stations, the agreement with the Wygnanski and Fiedler experiment is fairly satisfactory only for $x/D > 40$. The Wygnanski and Fiedler flow apparently does not approach self-preservation as quickly as do other reported jet experiments; the terms "fully developed" or "self-preserving" are questionable when applied to the Wygnanski and Fiedler experiment.

The predicted velocity profile (fig. 21(b)) is based on the local mixing-zone growth rate at $x/D = 60$. Compared with the experimental profile of Wygnanski and Fiedler, the half-velocity radius is well predicted, but the predicted profile is fuller near the center line; the predicted profile is closer to the empirical profile of Albertson et al. (ref. 25) in the high-speed half of the shear layer. The theoretical profile approaches zero velocity in the outer part of the shear layer more rapidly than does the experimental profile. The predicted TKE level (fig. 21(c)) agrees well with the Wygnanski and Fiedler experiment in the outer half of the profile, but the predicted center-line TKE level is about 13 percent below the experiment. It should be noted that the predicted TKE level is satisfactory in the region of peak shear stress. Predicted axial variations of R_T and the TKE profile parameter w are shown in figure 21(d). Even though the center-line velocity closely follows the x^{-1} decay (required for self-preservation) downstream of $x/D = 15$, R_T and w do not become constant until considerably farther downstream.

G.E. Heated Supersonic Jet – Test Case 19

This flow (test case 19) was computed by fitting a cosine profile to the velocity data at $x/D = 2.79$, and by using a fully developed initial shear stress. Agreement between predicted and experimental center-line velocity (fig. 22) is fairly satisfactory.

Paulk Jet in Moving Stream – Test Case 20

Even though the initial boundary layers are fairly thin in this flow (test case 20), the velocity ratio $(u_e/u_o = 0.48)$ exceeds that where a fully developed initial shear stress can be used. A potential core length of approximately 12D is predicted with the assumption of a fully developed initial R_T. The control volume initial region analysis was applied with $\delta_a = 0.082r_o$ and $\delta_j = 0.063r_o$. The experimental boundary-layer shapes are not well defined in reference 22; therefore, the initial region computations were carried out for two values of the velocity profile exponent $(n_a = n_j = 1/4$ and $n_a = n_j = 1/7)$. The result-

ing values of b, r_i, and shear stress were then used to start (at $x = 0$) the computations for the entire flow field. Both computations are shown in figure 23; the predicted flow field is obviously not very sensitive to the initial boundary-layer shape. Both predictions agree fairly well with the experimental center-line velocity but, of course, the experimental center-line concentration decays more rapidly than predicted.

It should be noted that the experimental values of $(u_c - u_e)/(u_o - u_e)$ were computed with $u_o = 390$ ft/sec (119 m/sec) and $u_e = 187$ ft/sec (57 m/sec), the observed values of u_o and u_e downstream in the flow field.

Chriss Hydrogen Jet in Moving Air Stream – Test Case 21

As with test case 10, this flow (test case 21) was computed (1) with experimental initial conditions, and (2) with fully developed R_T at $x = 0$. The initial shear stress for the first computation was taken from reference 22 at the most upstream axial station for which a shear stress was measured in this flow. The predicted center-line velocity agrees well with experiment (fig. 24(a)) but, as usual, the center-line composition decay is underpredicted. The computations which were started at $x = 0$ are shown in figure 24(b); the agreement with experiment is poor. Therefore, it can be concluded that the velocity ratio of this flow ($u_e/u_o = 0.31$) exceeds that for successful use of a fully developed initial shear stress.

Eggers Hydrogen Jet in Moving Air Stream – Test Case 22

As with test cases 11 and 12, this flow (test case 22) is wakelike in that the jet momentum flux is less than the outer stream momentum flux. The flow also has very thick initial boundary layers. In spite of the thick boundary layers and the velocity ratio $(u_e/u_j = 0.54)$, computations were started at $x = 0$ with a thin initial shear layer and with fully developed R_T. The predictions (fig. 25) are not as bad as could be expected, but the analysis does not predict qualitatively the behavior of the center-line velocity. It is unlikely that this flow will ever be properly predicted with an analysis which ignores the significant pressure gradients in the flow field.

CONCLUDING REMARKS

When the rather small investment of empirical information on turbulence structure is considered, the quality of the mean flow predictions is surprisingly good. Experience in computing a variety of flows has not indicated that the assumption of universal TKE profile shapes is grossly incorrect. The utility of the admittedly oversimplified model for turbulent dissipation has been significantly increased by relating the dissipation coefficient a_2 to the local turbulent Reynolds number.

A persistent point of criticism about TKE methods for free shear flows has been that the required detailed information on initial conditions is not generally available for engineering flows. Experience has shown that a considerable number of practical flows can be computed without detailed information on the initial conditions. For u_e/u_o less than 0.25, specifying a fully developed initial shear stress works very well. Wakelike flows, such as test case 12, seem to be fairly insensitive to initial conditions. For jet flows with velocity ratio u_e/u_o greater than 0.25, the control volume initial region analysis shows promise. The very limited experience with this initial region analysis for constant density flows has indicated that the results are not overly sensitive to the initial boundary-layer characteristics; good guesses about the initial boundary layers seem to be sufficient.

Turbulent kinetic energy methods, of which this method is a simplified example, represent a fundamental improvement over eddy-viscosity models in that more of the physics of the turbulent motion is taken into account, albeit crudely. It appears that these methods have been developed to the point where they are routinely applicable to engineering calculations on a broad class of free turbulent flows.

REFERENCES

1. Peters, C. E.; Phares, W. J.; and Cunningham, T. H. M.: Theoretical and Experimental Studies of Ducted Mixing and Burning of Coaxial Streams. J. Spacecraft Rockets, vol. 6, no. 12, Dec. 1969, pp. 1435-1441.

2. Peters, C. E.: Turbulent Mixing and Burning of Coaxial Streams Inside a Duct of Arbitrary Shape. AEDC-TR-68-270, U.S. Air Force, Jan. 1969. (Available from DDC as AD 680 397.)

3. Donaldson, Coleman duP.; and Gray, K. Evan: Theoretical and Experimental Investigation of the Compressible Free Mixing of Two Dissimilar Gases. AIAA J., vol. 4, no. 11, Nov. 1966, pp. 2017-2025.

4. Harsha, Philip Thomas: Free Turbulent Mixing: A Critical Evaluation of Theory and Experiment. AEDC-TR-71-36, U.S. Air Force, Feb. 1971. (Available from DDC as AD 718 956.)

5. Bradshaw, P.; Ferriss, D. H.; and Atwell, N. P.: Calculation of Boundary-Layer Development Using the Turbulent Energy Equation. J. Fluid Mech., vol. 28, pt. 3, May 26, 1967, pp. 593-616.

6. Lee, S. C.; and Harsha, P. T.: Use of Turbulent Kinetic Energy in Free Mixing Studies. AIAA J., vol. 8, no. 6, June 1970, pp. 1026-1032.

7. Laster, M. L.: Inhomogeneous Two-Stream Turbulent Mixing Using the Turbulent Kinetic Energy Equation. AEDC-TR-70-134, U.S. Air Force, May 1970. (Available from DDC as AD 705 578.)

8. Patankar, S. V.; and Spalding, D. B.: A Finite-Difference Procedure for Solving the Equations of the Two-Dimensional Boundary Layer. Int. J. Heat Mass Transfer, vol. 10, no. 10, Oct. 1967, pp. 1389-1411.

9. Heck, P. H.; and Ferguson, D. R.: Analytical Solution for Free Turbulent Mixing in Compressible Flows. AIAA Paper No. 71-4, Jan. 1971.

10. Ortwerth, P. J.: Mechanism of Mixing of Two Nonreacting Gases. AFAPL-TR-71-18, U.S. Air Force, Oct. 1971.

11. Ortwerth, P. J.: Mechanism of Mixing of Two Nonreacting Gases. AIAA Paper No. 71-725, June 1971.

12. Harsha, P. T.; and Lee, S. C.: Correlation Between Turbulent Shear Stress and Turbulent Kinetic Energy. AIAA J., vol. 8, no. 8, Aug. 1970, pp. 1508-1510.

13. Spencer, Bruce Walton: Statistical Investigation of Turbulent Velocity and Pressure Fields in a Two-Stream Mixing Layer. Ph. D. Thesis, Univ. of Illinois, 1970.

14. Liepmann, Hans Wolfgang; and Laufer, John: Investigation of Free Turbulent Mixing. NACA TN 1257, 1947.

15. Pindell, Robert George: An Experimental Study of the Coaxial Turbulent Jet. Ph. D. Dissertation, North Carolina State Univ., 1970.

16. Wygnanski, I.; and Fiedler, H.: Some Measurements in the Self-Preserving Jet. J. Fluid Mech., vol. 38, pt. 3, Sept. 18, 1969, pp. 577-612.

17. Sami, Sedat: Velocity and Pressure Fields of a Diffusing Jet. Ph. D. Dissertation, Univ. of Iowa, 1966.

18. Sami, S.; Carmody, Thomas; and Rouse, Hunter: Jet Diffusion in the Region of Flow Establishment. J. Fluid Mech., vol. 27, pt. 2, Feb. 2, 1967, pp. 231-252.

19. Bradshaw, P.; Ferriss, D. H.; and Johnson, R. F.: Turbulence in the Noise-Producing Region of a Circular Jet. J. Fluid Mech., vol. 19, pt. 4, Aug. 1964, pp. 591-624.

20. Warren, Walter R.: An Analytical and Experimental Study of Compressible Free Jets. Ph. D. Dissertation, Princeton Univ., 1957.

21. Spalding, D. B.; and Chi, S. W.: The Drag of a Compressible Turbulent Boundary Layer on a Smooth Flat Plate With and Without Heat Transfer. J. Fluid Mech., vol. 18, pt. 1, Jan. 1964, pp. 117-143.

22. Chriss, D. E.; and Paulk, R. A.: An Experimental Investigation of Subsonic Coaxial Free Turbulent Mixing. AEDC-TR-71-236, AFOSR-72-0237 TR, U.S. Air Force, Feb. 1972. (Available from DDC as AD 737 098.)

23. Chevray, R.: The Turbulent Wake of a Body of Revolution. Trans. ASME, Ser. D: J. Basic Eng., vol. 90, no. 2, June 1968, pp. 275-284.

24. Demetriades, Anthony: Mean-Flow Measurements in an Axisymmetric Compressible Turbulent Wake. AIAA J., vol. 6, no. 3, Mar. 1968, pp. 432-439.

25. Albertson, M. L.; Dai, Y. B.; Jensen, R. A.; and Rouse, Hunter: Diffusion of Submerged Jets. Paper No. 2409, Transactions Amer. Soc. Civil Eng., vol. 115, 1950, pp. 639-664.

TABLE I.- INITIAL CONDITIONS FOR THE EXPERIMENTAL FLOWS

Test case	Flow	x_1	b_1	r_{i1}	$R_{T,1}$	Notes
6	Maestrello and McDaid axisymmetric jet, $M_o = 0.64$	$2r_o$	$0.87r_o$	$0.52r_o$	190	Experimental profile, fully developed R_T
		0	$.01r_o$	$.86r_o$	190	r_o corrected for momentum
						Fully developed R_T
7	Eggers supersonic jet, $M_o = 2.22$	0	$.01r_o$	r_o	283	Fully developed R_T
8	G.E. heated jet, $M_o = 0.7$	$5.58r_o$	$1.70r_o$	$.18r_o$	212	Experimental profile, fully developed R_T
9	Forstall jet in moving stream, $u_e/u_o = 0.25$	0	$.01r_o$	$.88r_o$	143	r_o corrected for momentum
						Fully developed R_T
10	Chriss H_2 jet in air stream, $u_e/u_o = 0.16$	$5.94r_o$	$1.132r_o$	$.412r_o$	98.3	Experimental profile and R_T
		0	$.01r_o$	r_o	120	Fully developed R_T
11	Eggers and Torrence jet in moving stream	0	$.01r_o$	r_o	130	Fully developed R_T
12	Eggers H_2 jet in air stream, $M_e = 1.33$	0	$.01r_o$	r_o	125	Fully developed R_T
15	Chevray axisymmetric wake	0	.0257D	0	1930	Equivalent cosine profile, $u_c = 0.083u_e$
17	Demetriades axisymmetric wake, $M_e = 3$	17D	1.00D	0	48	Experimental profile. R_T quoted by Demetriades
18	Fully developed axisymmetric jet	0	$.01r_o$	r_o	143	Fully developed R_T
19	G.E. heated jet, $M_o = 1.36$	$5.58r_o$	$1.30r_o$	$.46r_o$	238	Experimental profile, fully developed R_T
20	Paulk jet in moving stream, $u_e/u_o = 0.48$	0	$.113r_o$	$.916r_o$	36.8	Initial condition analysis, $n_a = n_j = 1/4$
		0	$.122r_o$	$.923r_o$	42.9	Initial condition analysis, $n_a = n_j = 1/7$
21	Chriss H_2 jet in air stream, $u_e/u_o = 0.31$	$5.15r_o$	$1.17r_o$	$.464r_o$	48.2	Experimental profile and R_T
		0	$.01r_o$	r_o	130	Fully developed R_T
22	Eggers H_2 jet in air stream, $M_e = 2.5$	0	$.01r_o$	r_o	110	Fully developed R_T

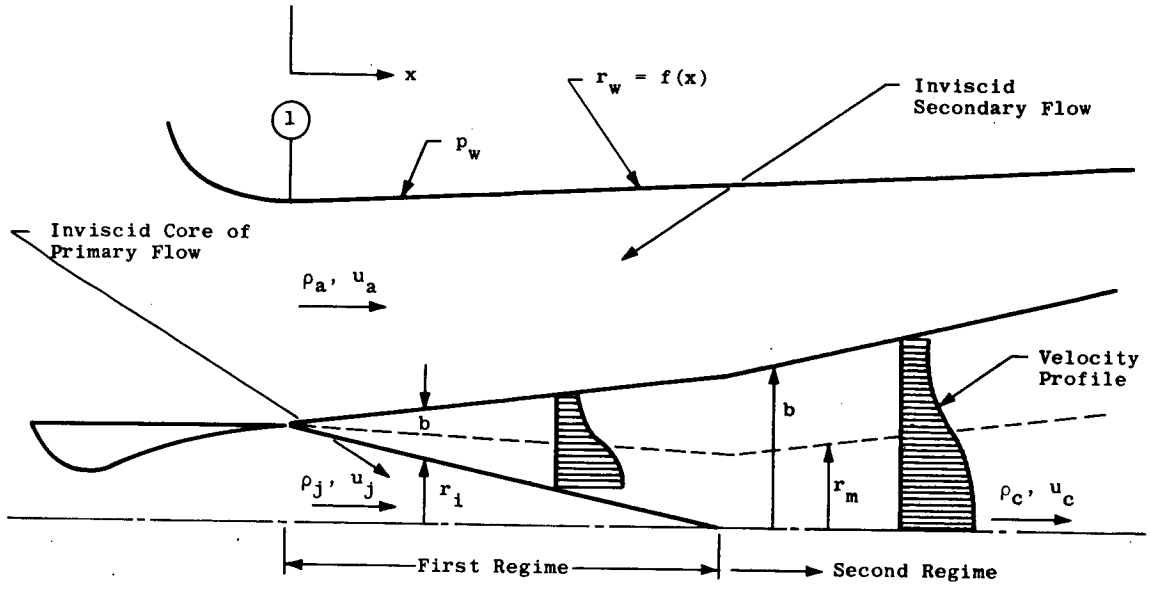

Figure 1.- Nomenclature for integral analysis.

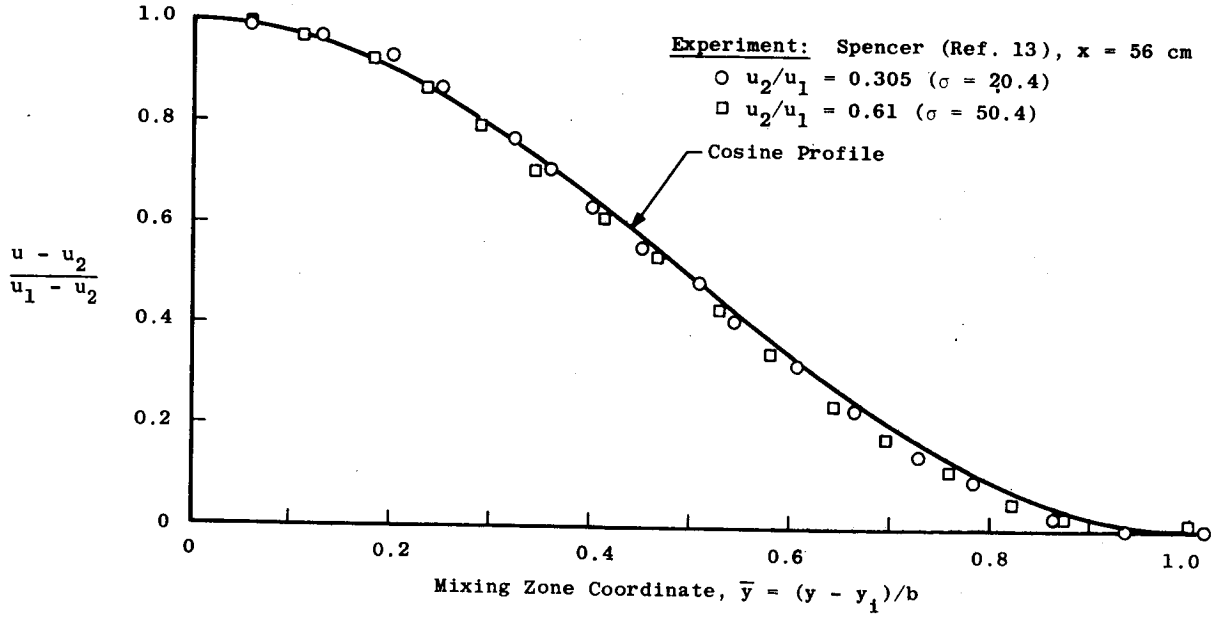

Figure 2.- Near-field velocity profile.

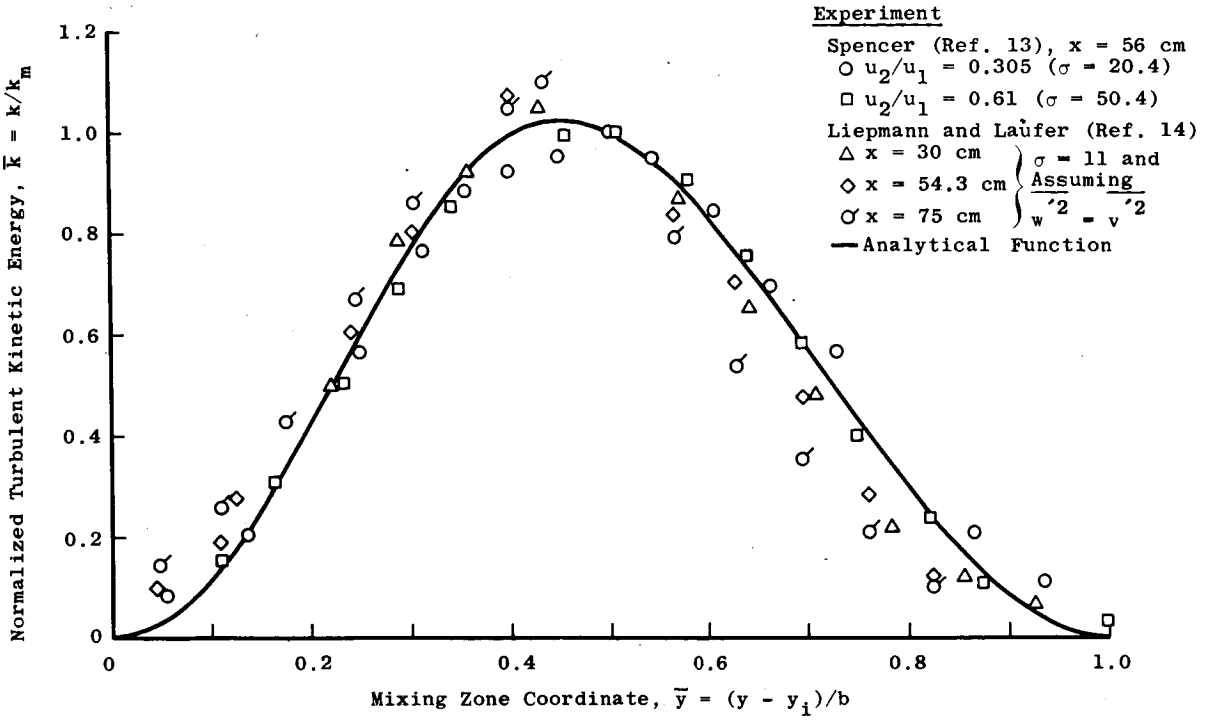

Figure 3.- Near-field turbulent kinetic energy profile.

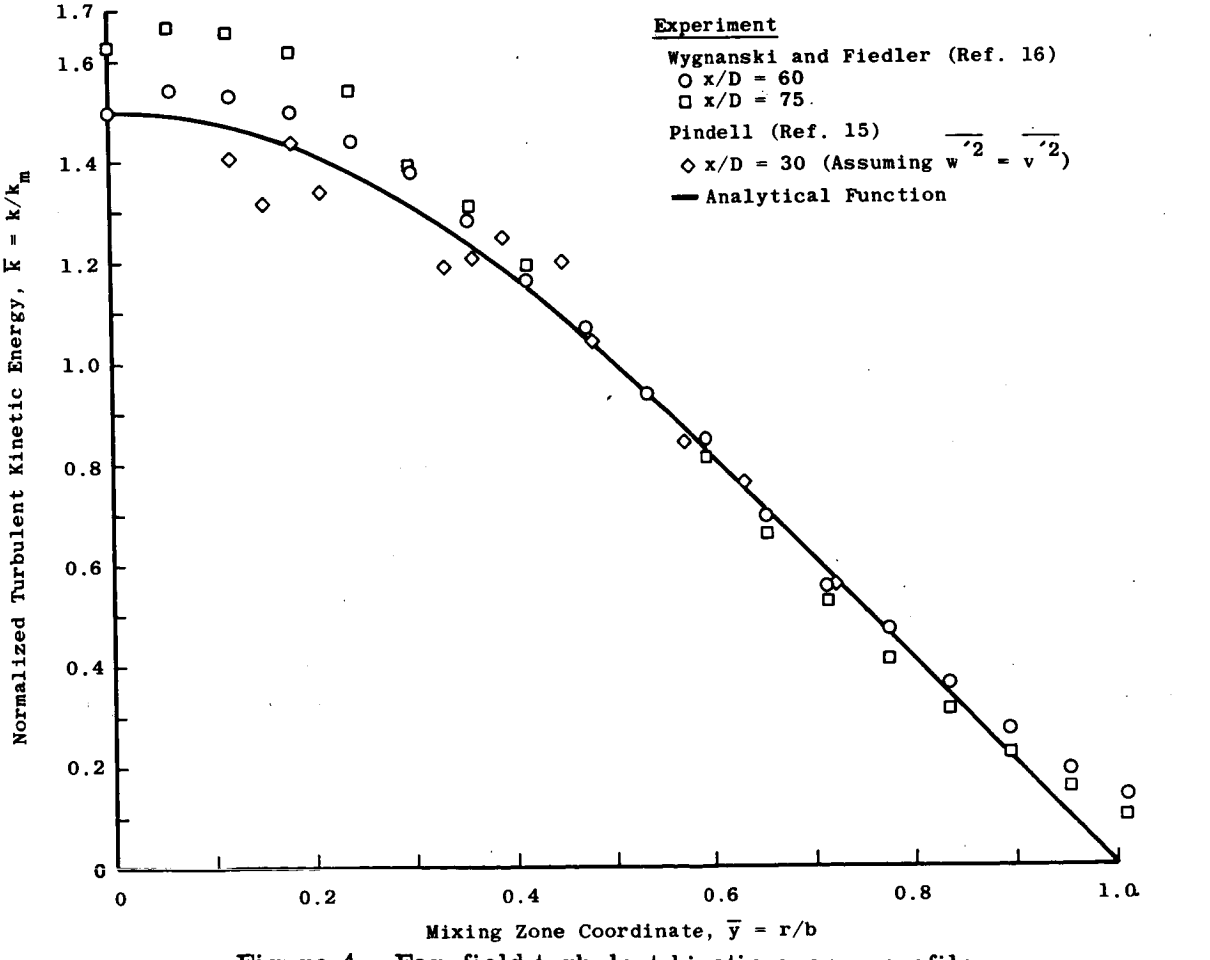

Figure 4.- Far-field turbulent kinetic energy profile.

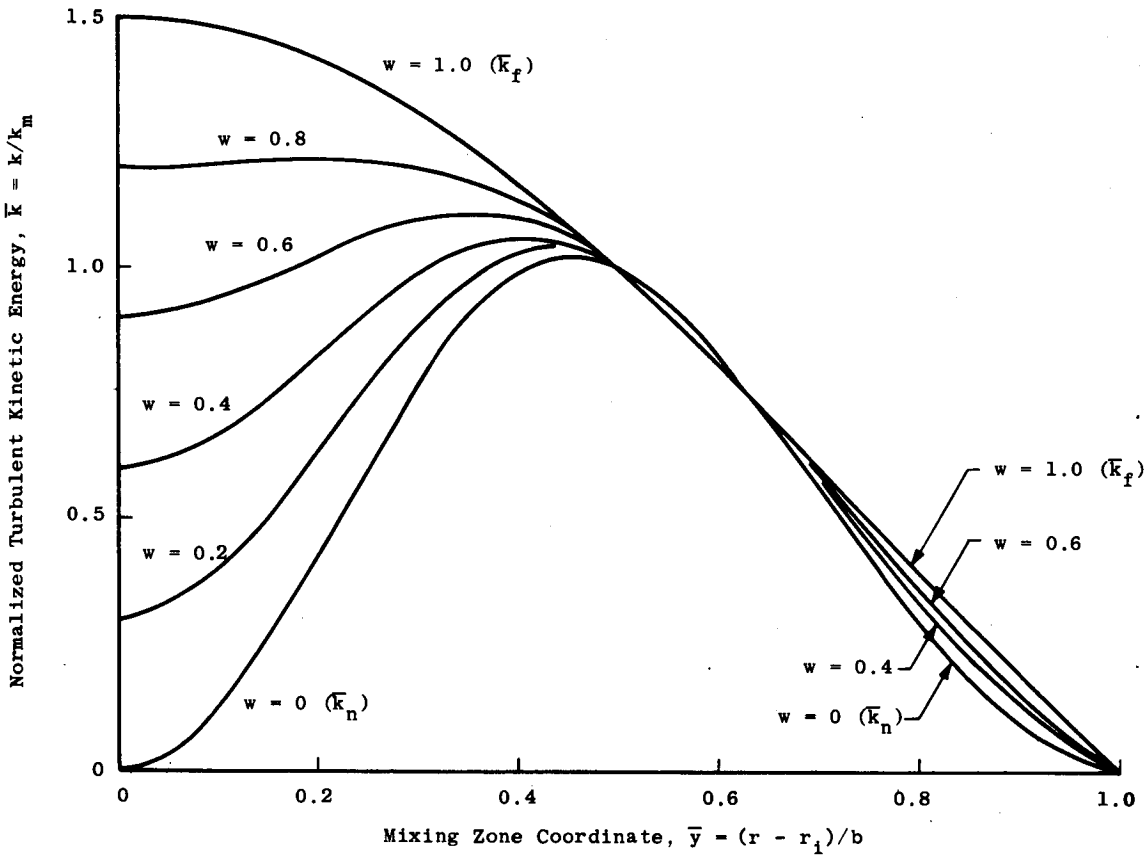

Figure 5.- Family of turbulent kinetic energy profiles.

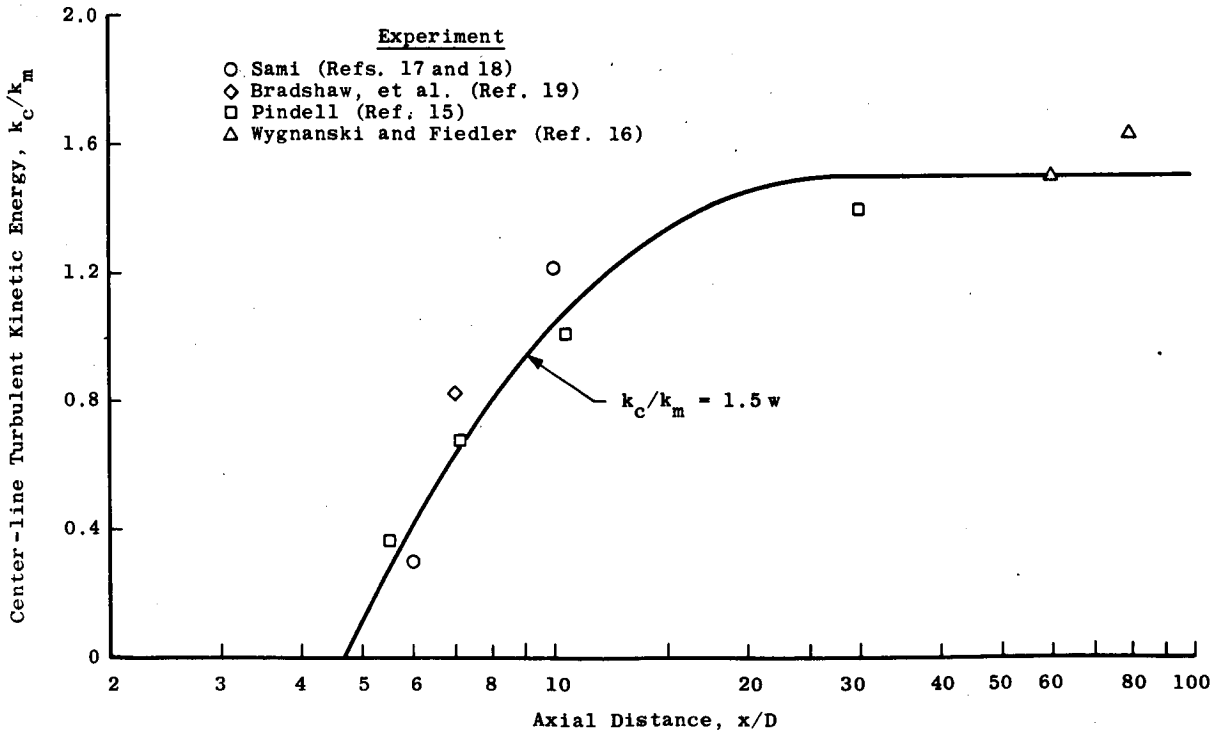

Figure 6.- Center-line turbulent kinetic energy for axisymmetric jet into still air.

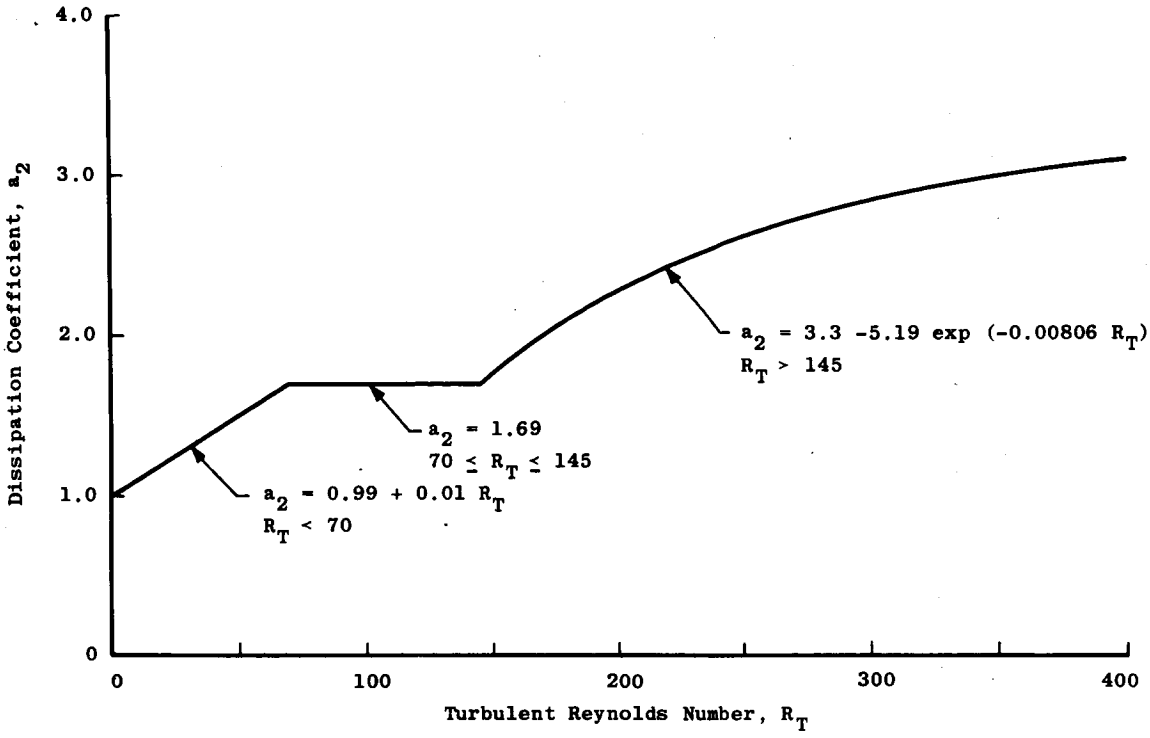

Figure 7.- Dissipation coefficient as a function of turbulent Reynolds number.

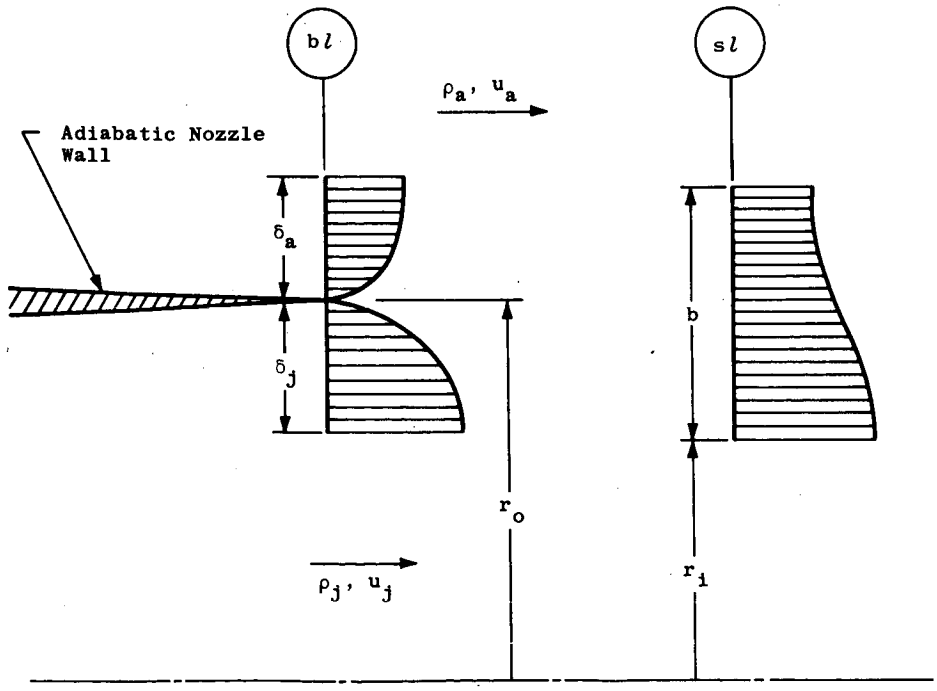

Figure 8.- Nomenclature for initial region analysis. *sl* and *bl* denote shear layer and boundary layer.

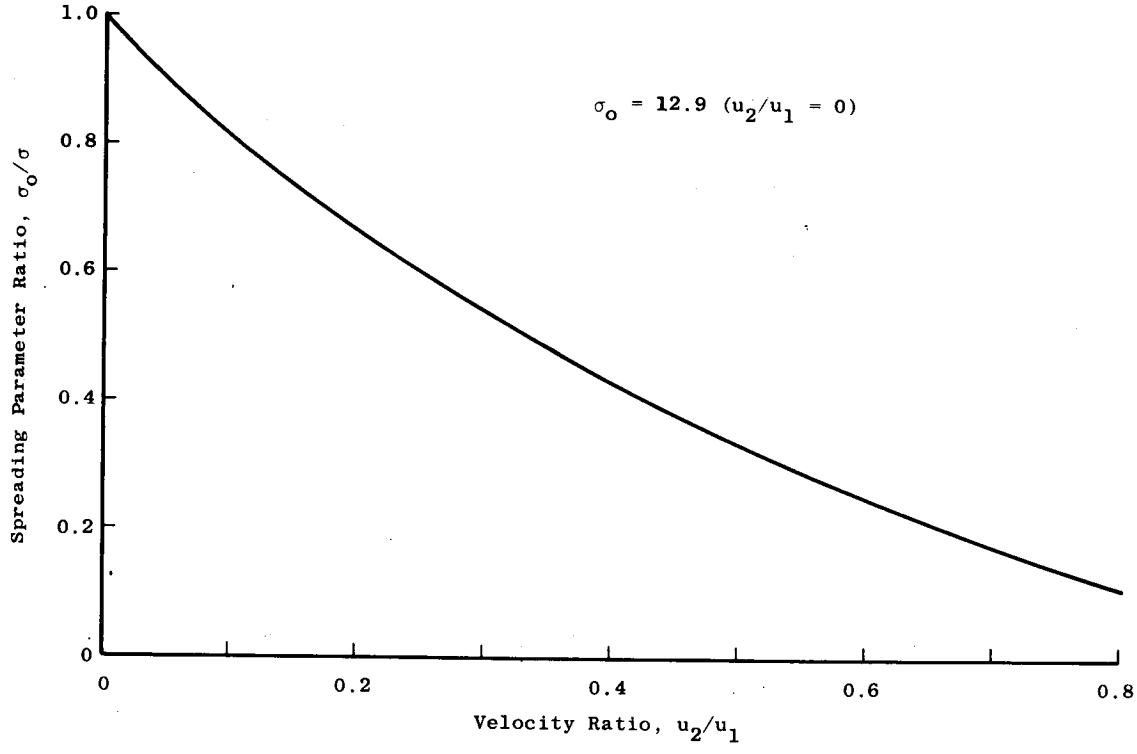

Figure 9.- Test case 1 – Effect of velocity ratio on growth of constant-density two-dimensional fully developed shear layer.

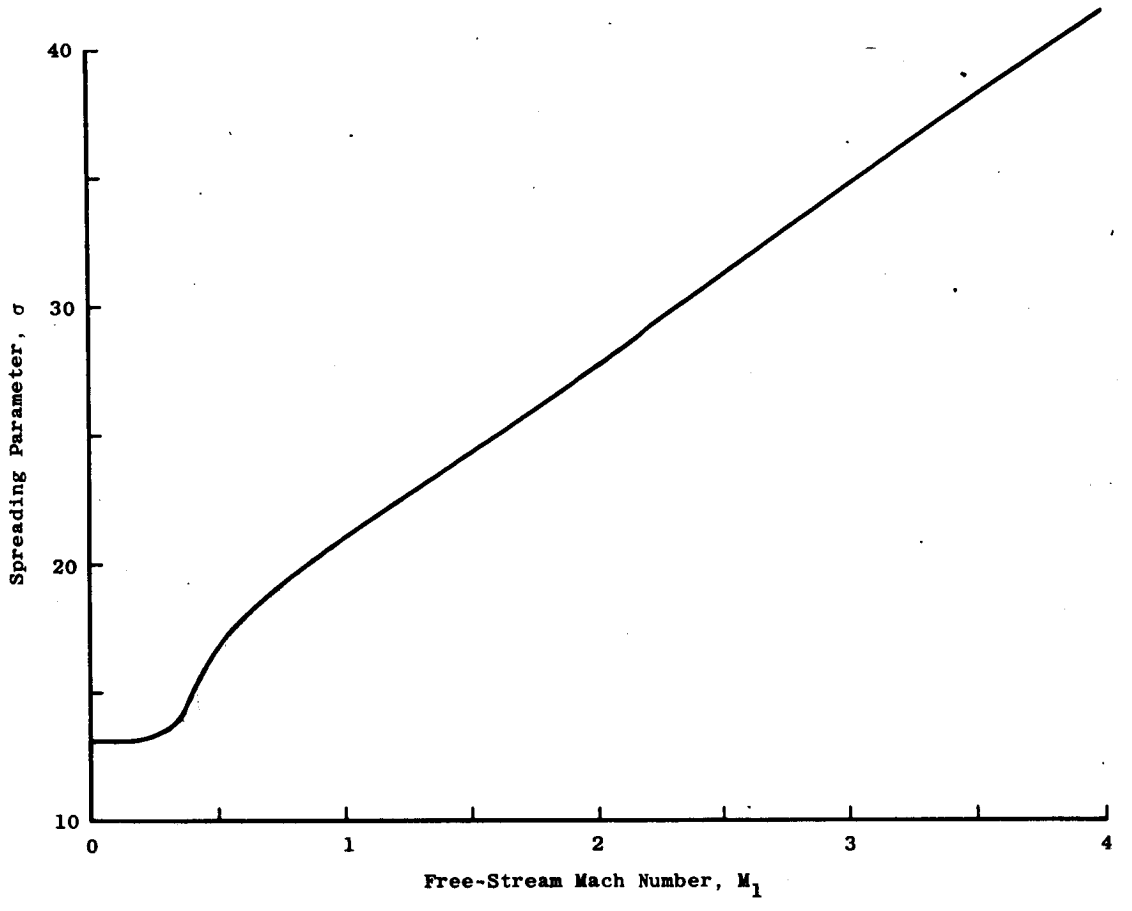

(a) Variation of σ with Mach number.

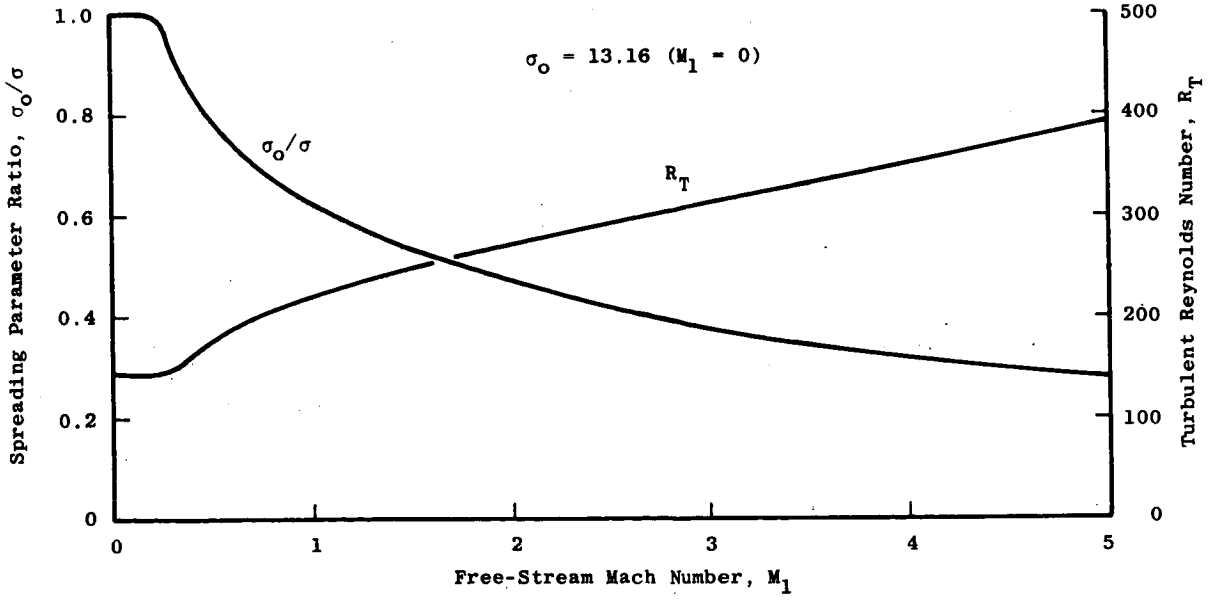

(b) Variation of σ_o/σ and R_T with Mach number.

Figure 10.- Test case 2 – Effect of Mach number on fully developed spreading parameter.

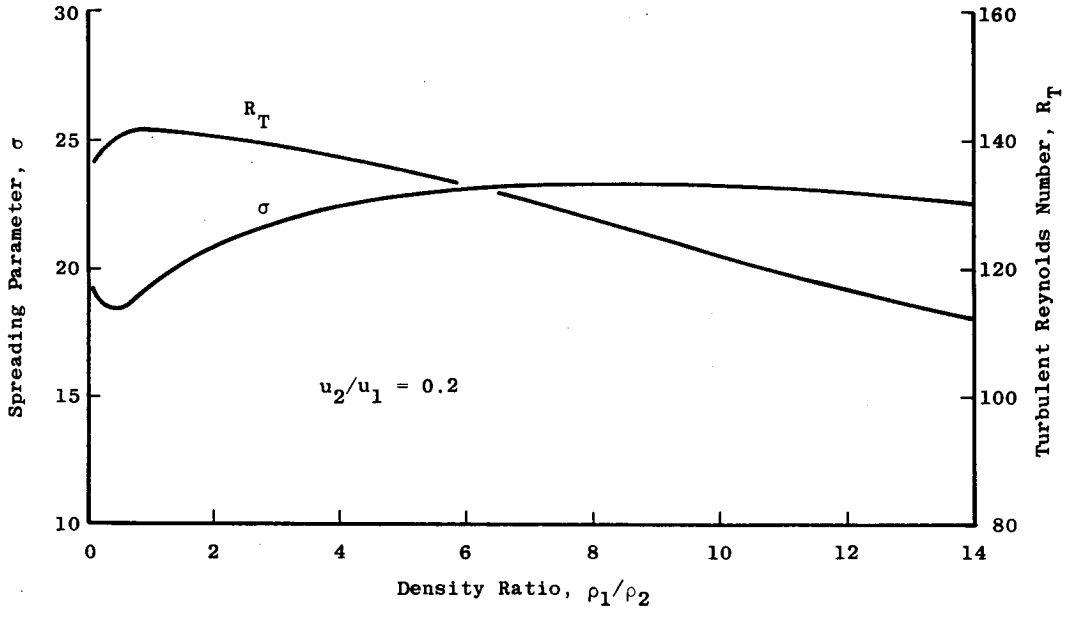

Figure 11.- Test case 3 – Effect of density ratio on growth rate of fully developed two-dimensional shear layer.

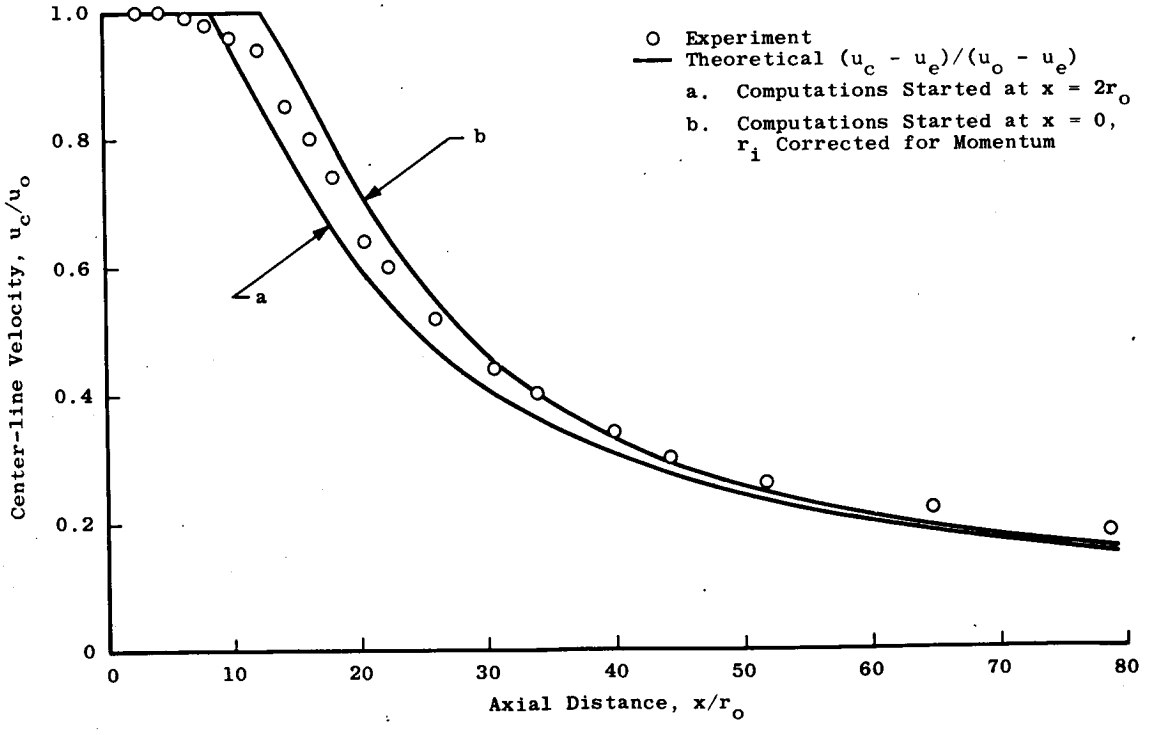

Figure 12.- Test case 6 – Maestrello and McDaid axisymmetric jet into still air. $M_o = 0.64$.

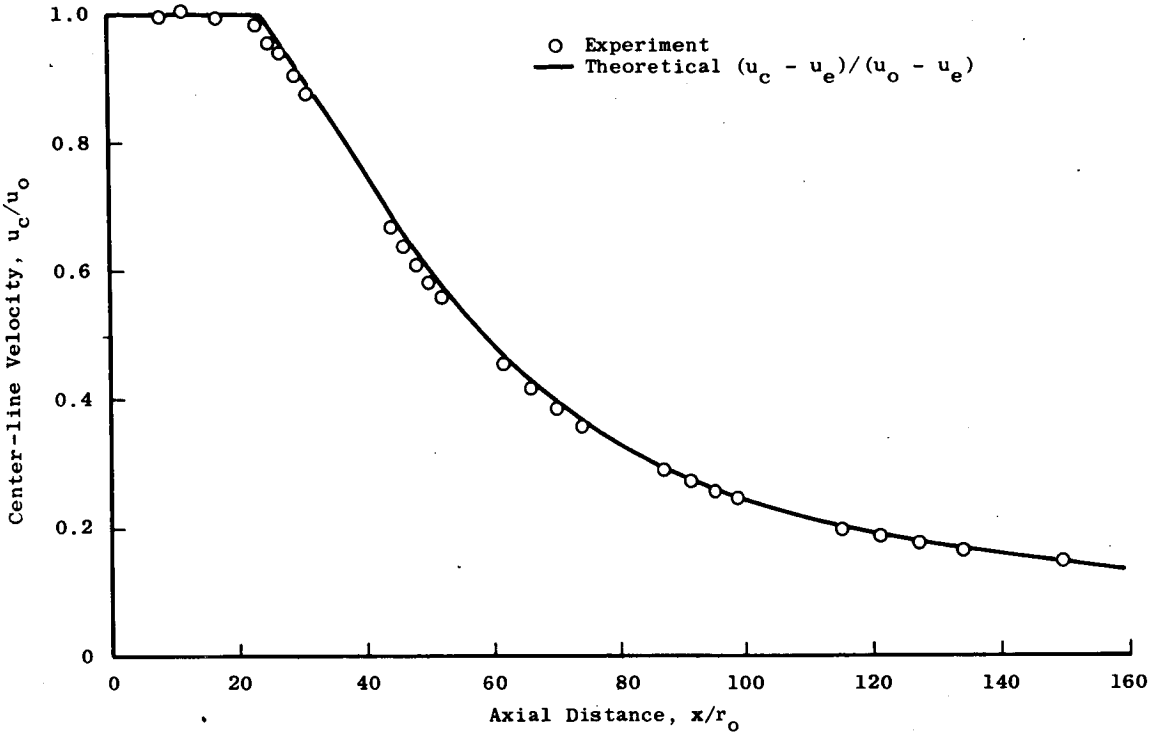

(a) Center-line velocity decay.

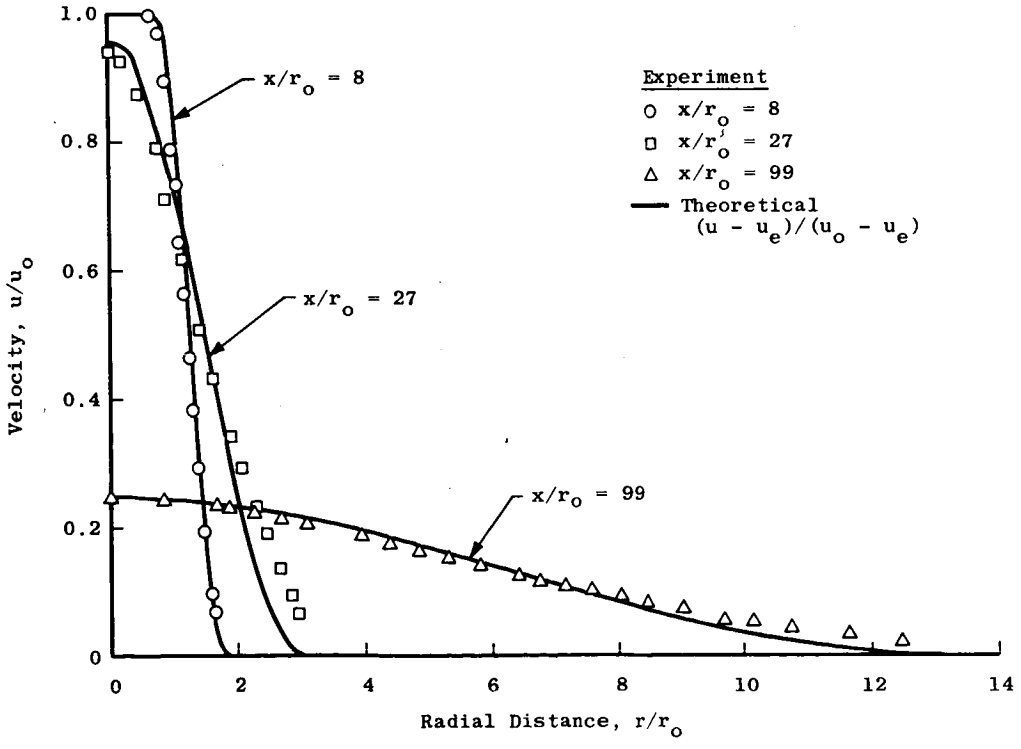

(b) Radial velocity profiles.

Figure 13.- Test case 7 – Eggers axisymmetric jet into still air. M_O = 2.22.

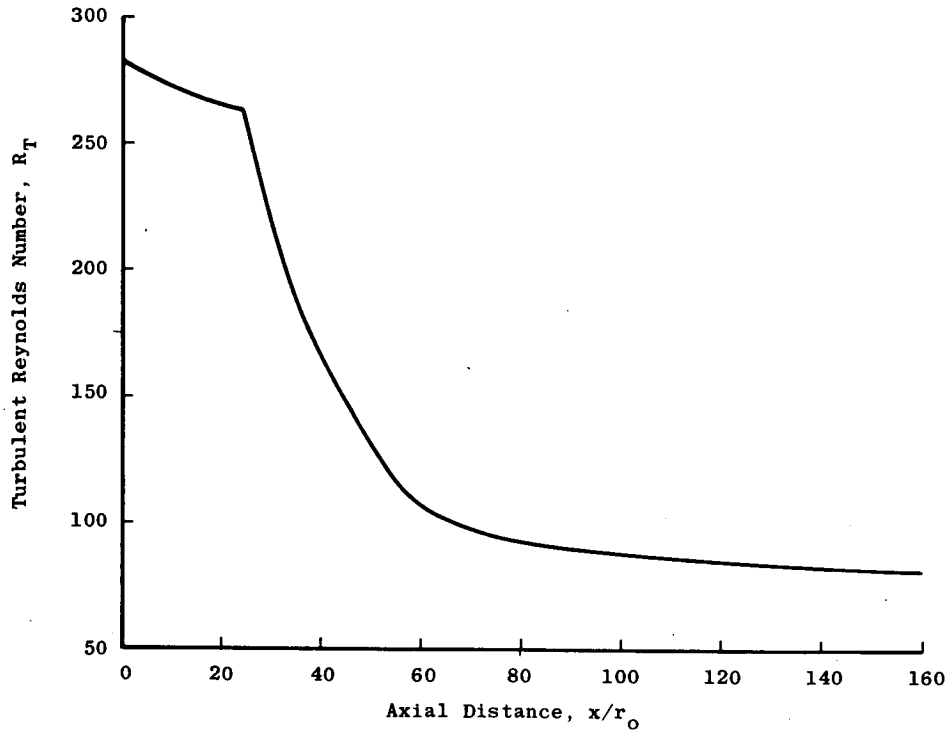

(c) Variation of R_T with x/r_o.

Figure 13.- Concluded.

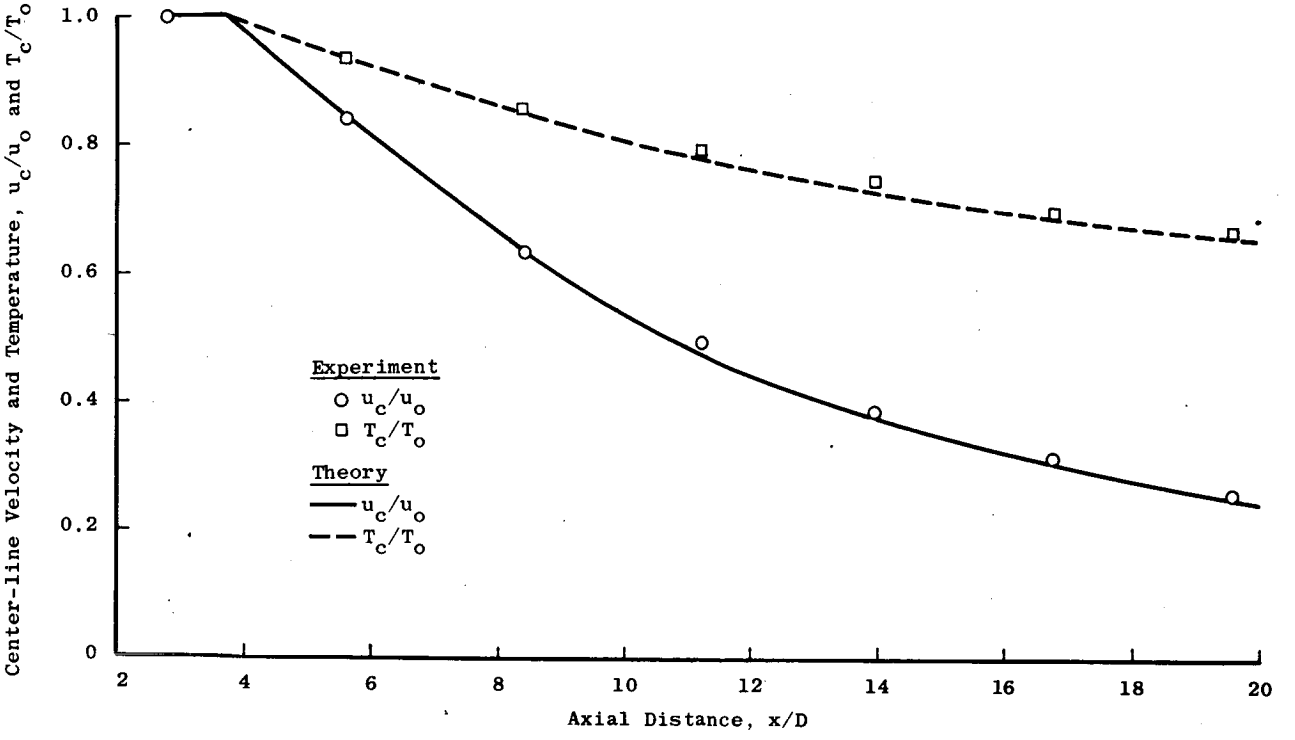

Figure-14.- Test case 8 – Heated axisymmetric jet. $M_o = 0.7$.

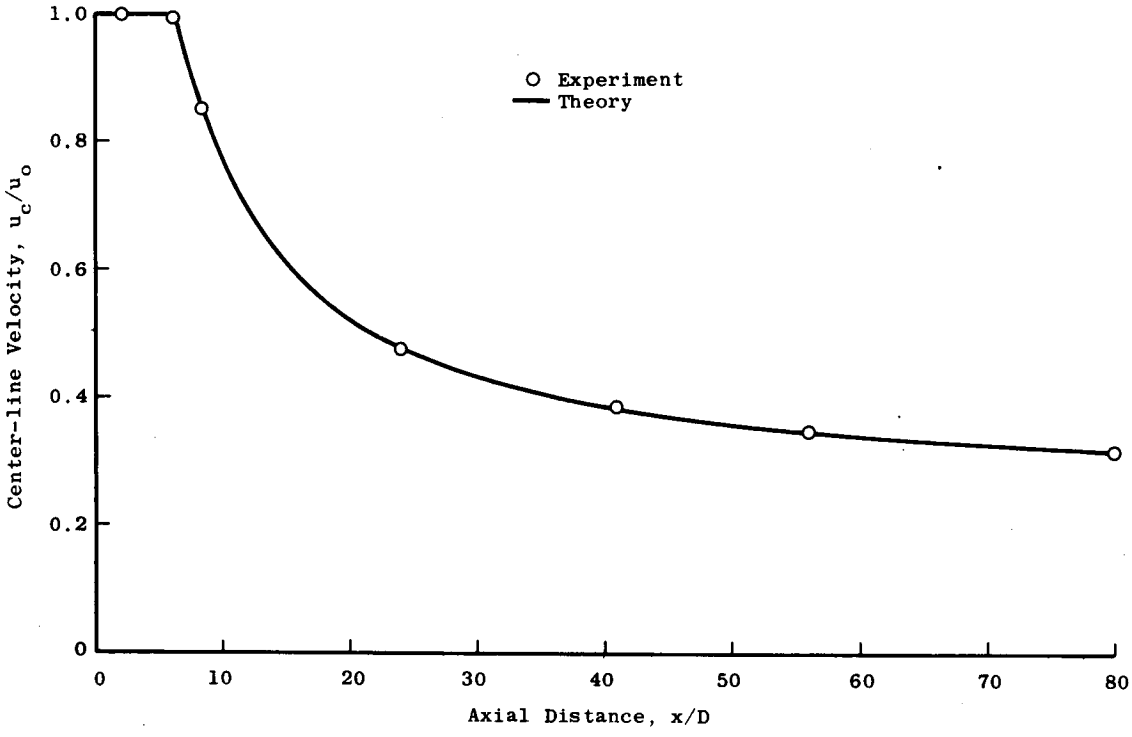

(a) Center-line velocity.

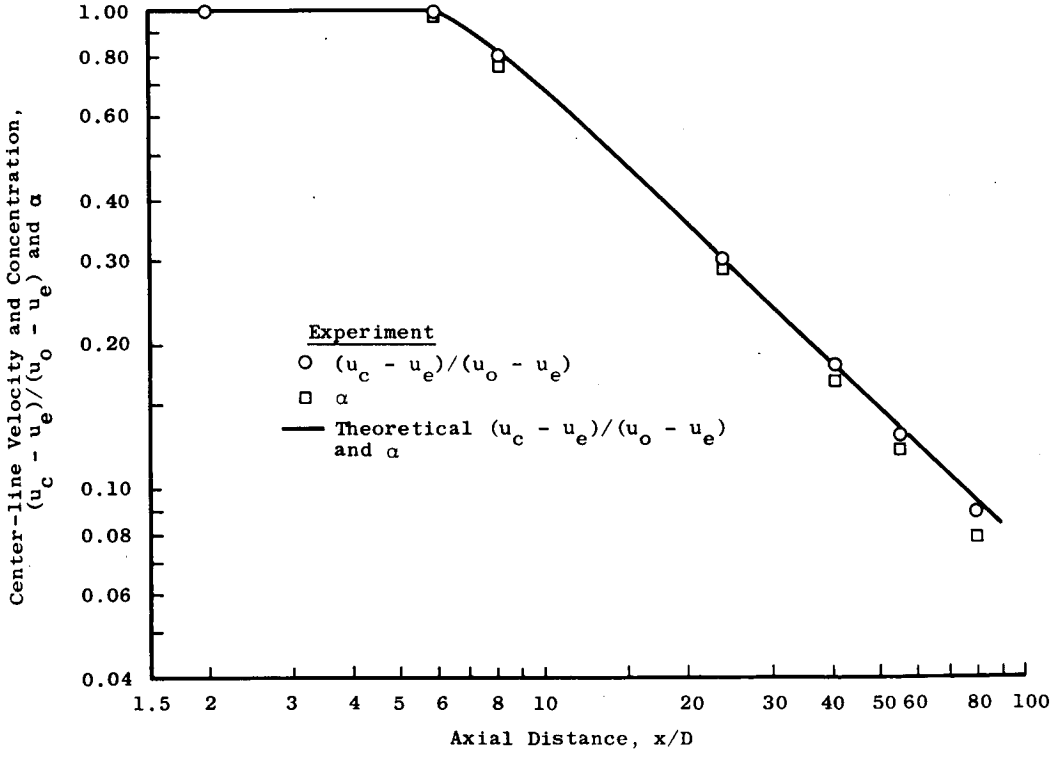

(b) Log plot of center-line velocity and concentration.

Figure 15.- Test case 9 – Forstall axisymmetric jet in moving stream. $u_e/u_o = 0.25$.

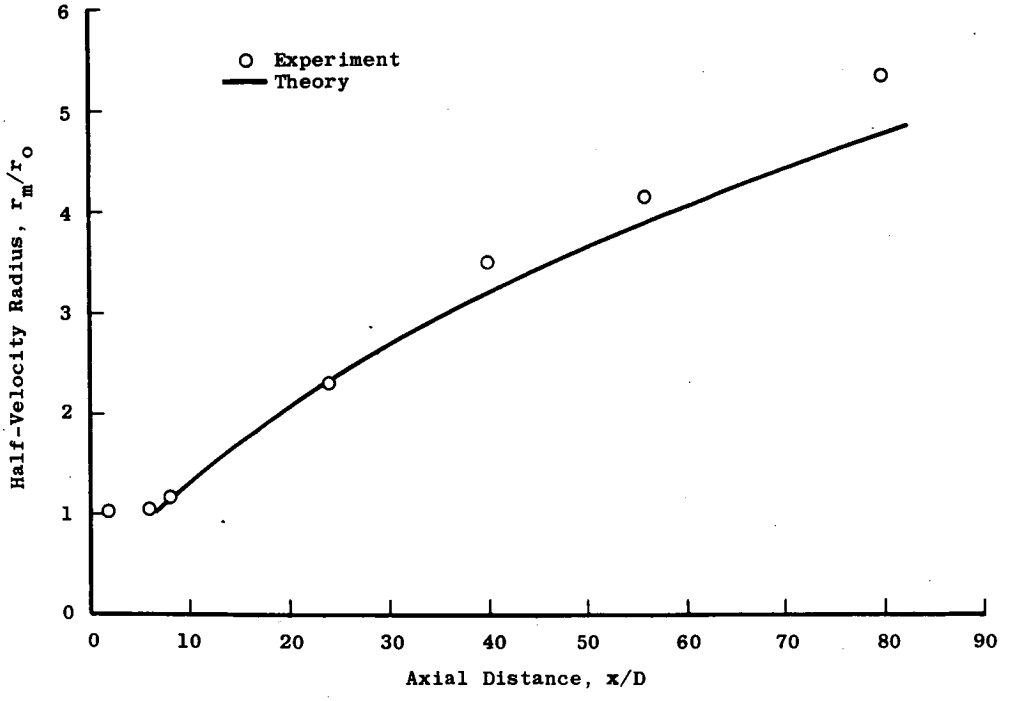

(c) Half-velocity radius.

Figure 15.- Concluded.

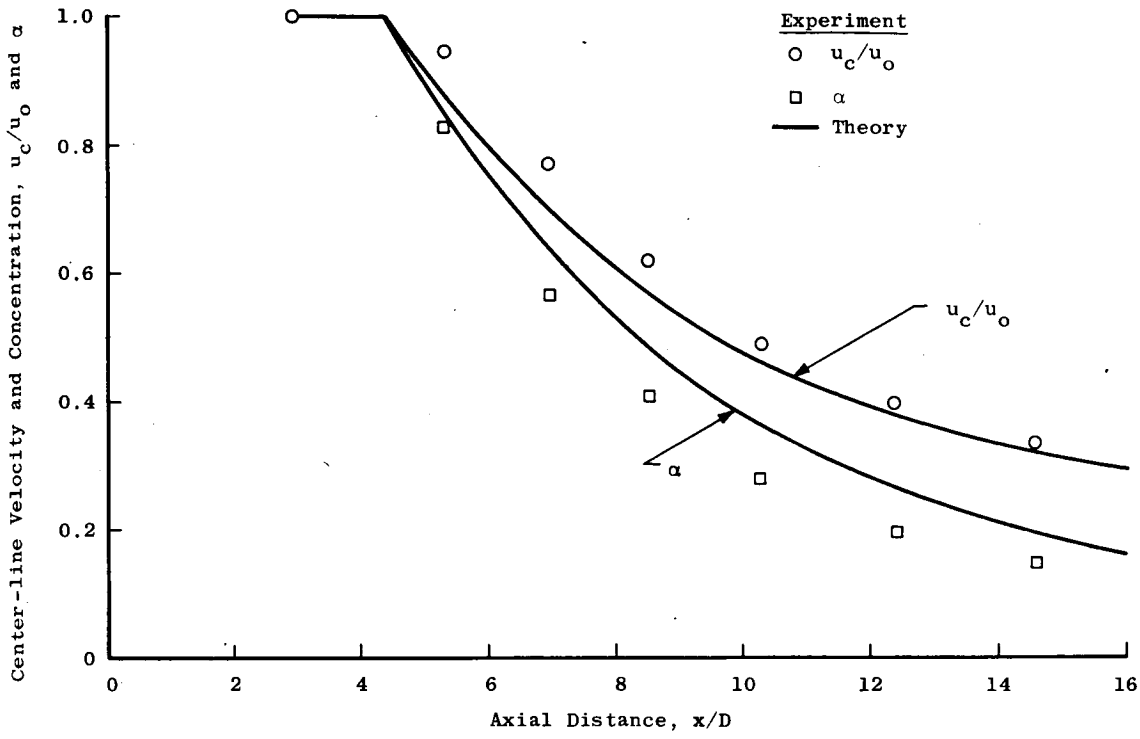

(a) Computations started at x/D = 2.97.

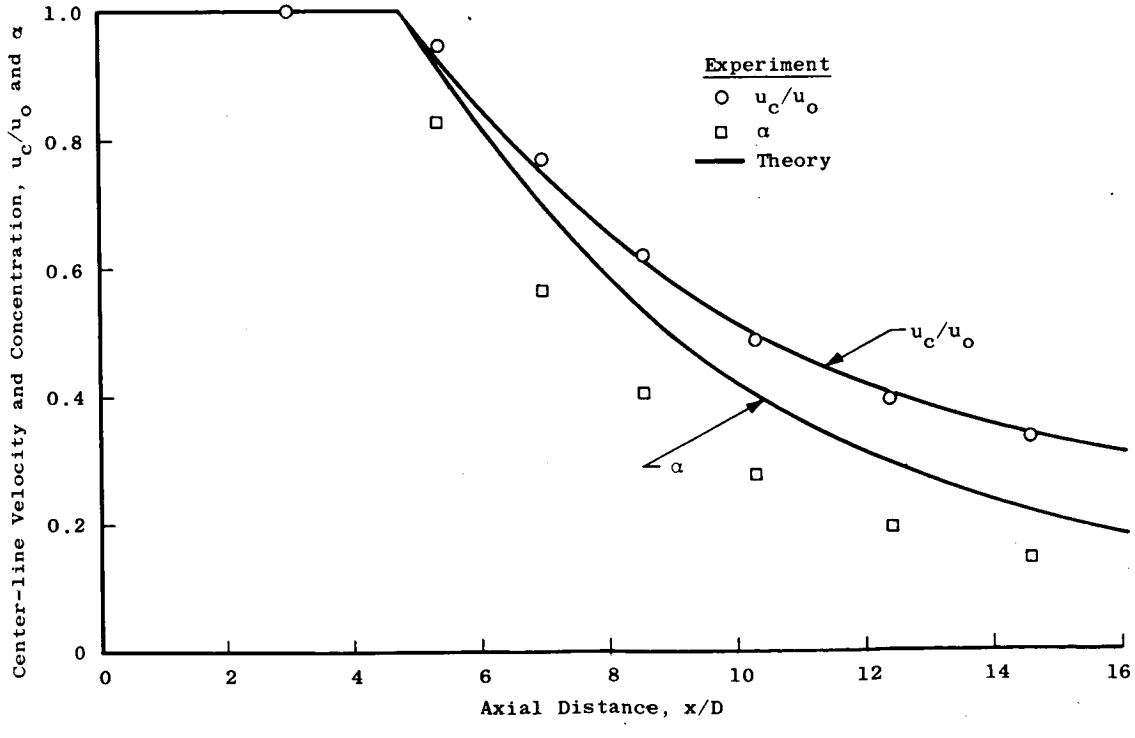

(b) Computations started at x = 0.

Figure 16.- Test case 10 – Chriss H_2 jet in moving stream. $u_e/u_o = 0.16$.

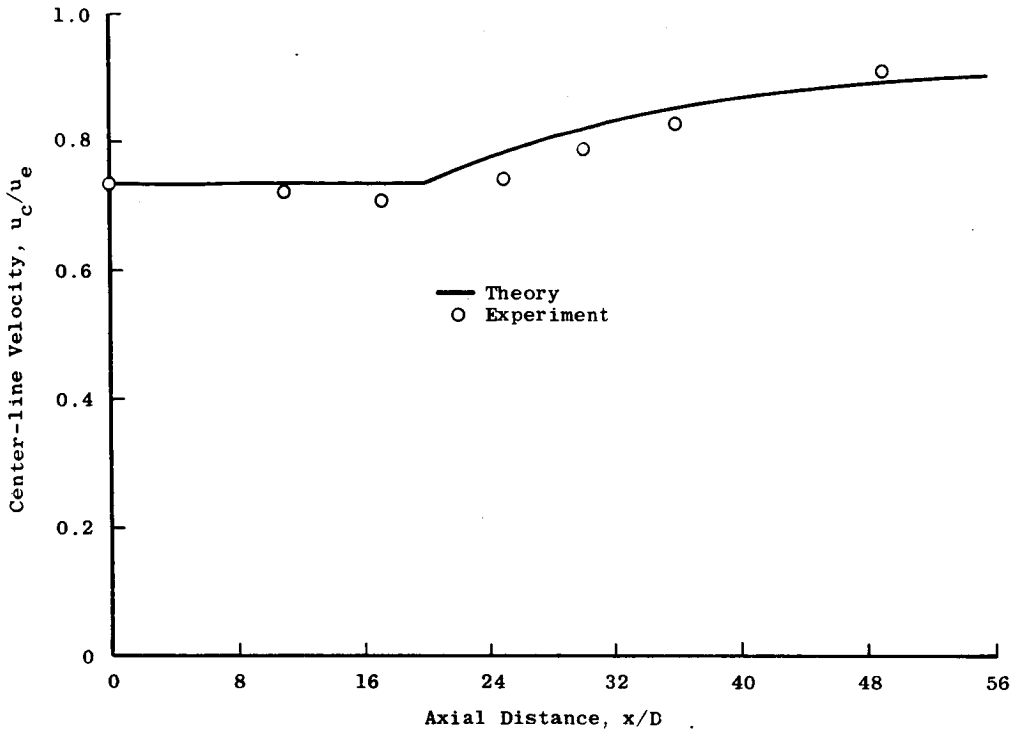

Figure 17.- Test case 11 – Eggers and Torrence axisymmetric jet in a moving stream.

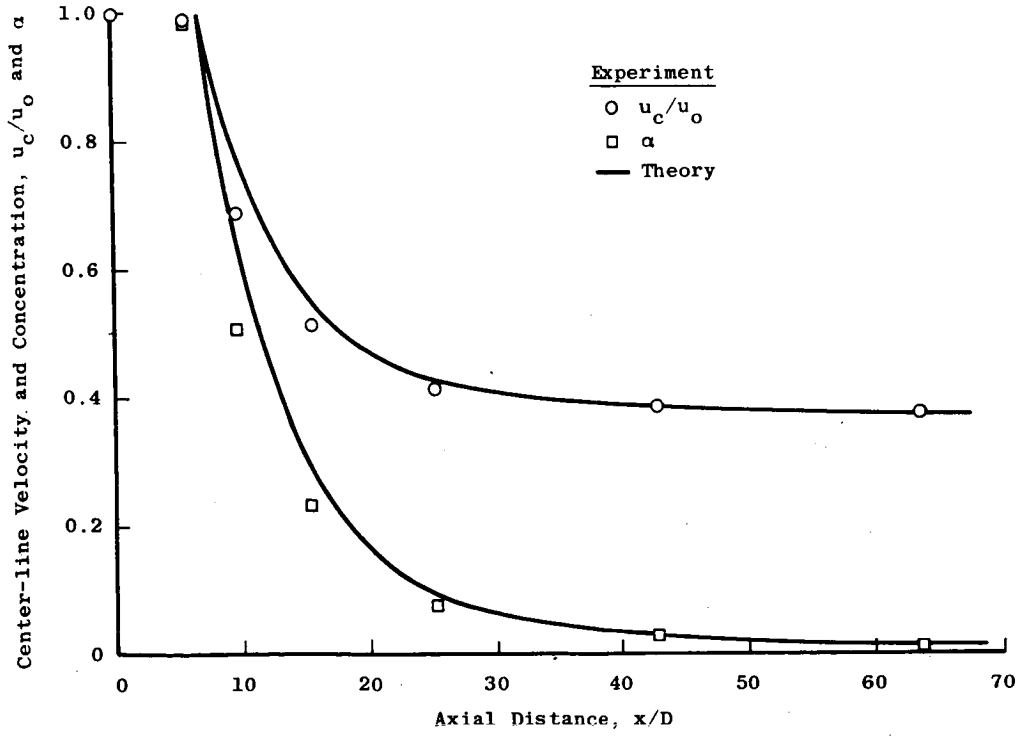

Figure 18.- Test case 12 – Eggers H_2 jet in moving stream. $M_e = 1.33$.

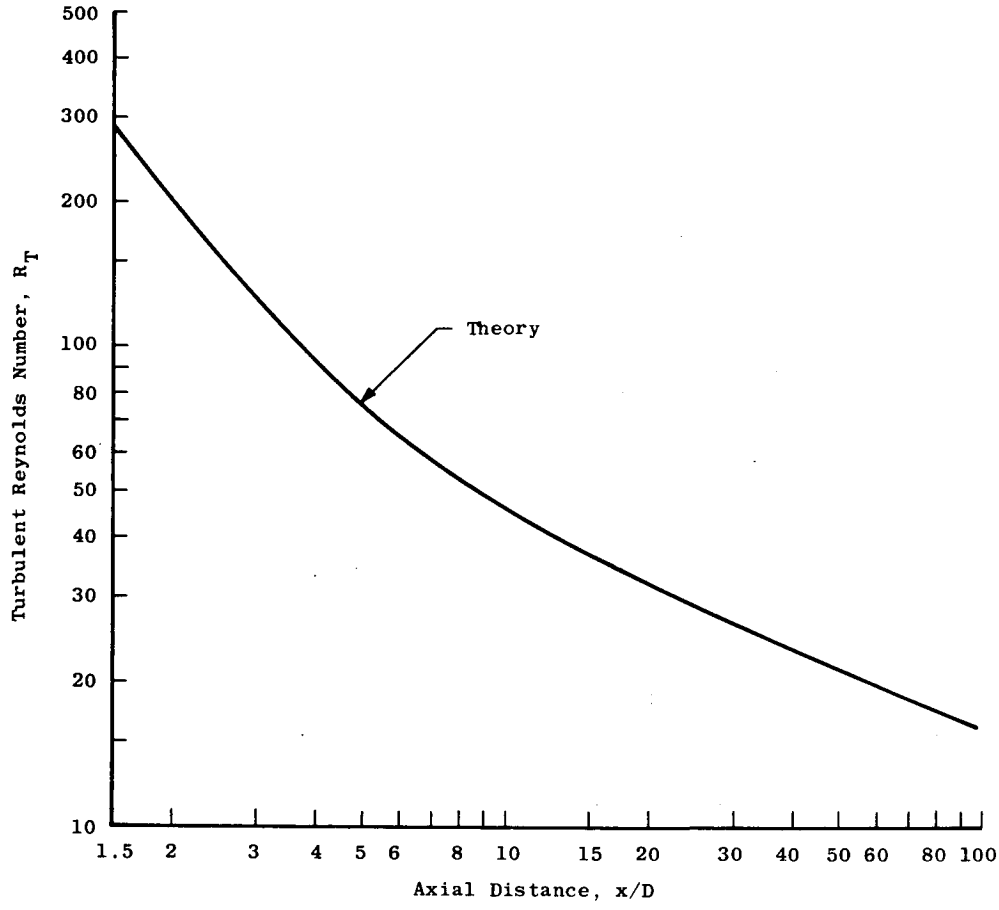

(c) Variation of R_T with x/D.

Figure 19.- Concluded.

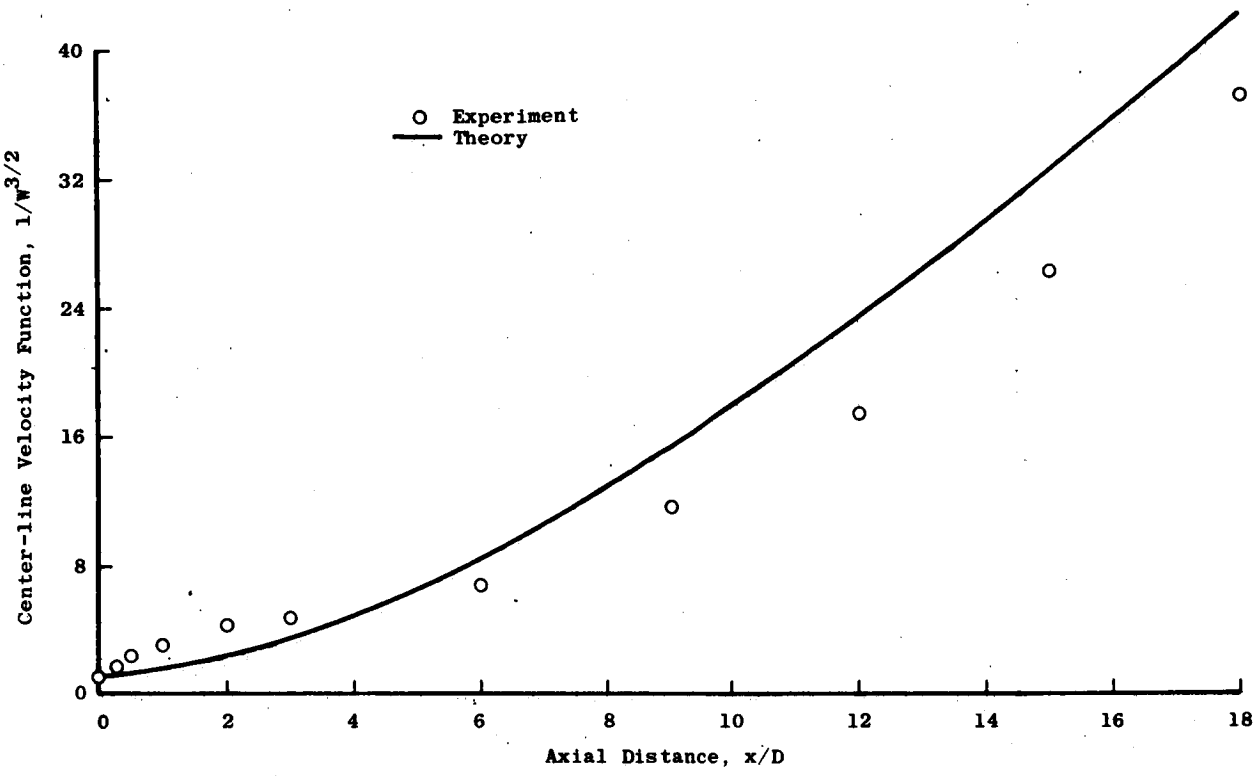

(a) Variation of $1/W^{3/2}$ with x/D.

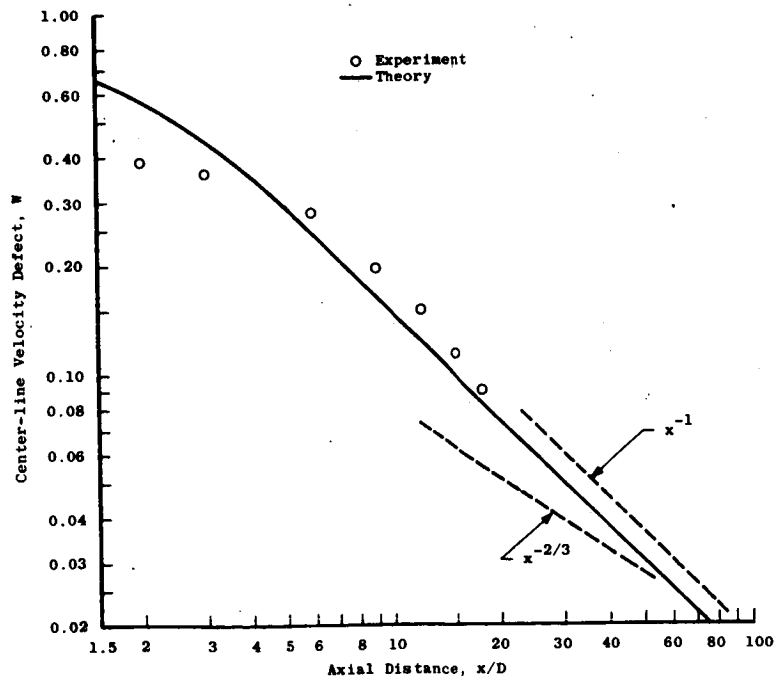

(b) Log plot of W against x/D.

Figure 19.- Test case 15 – Chevray axisymmetric wake.

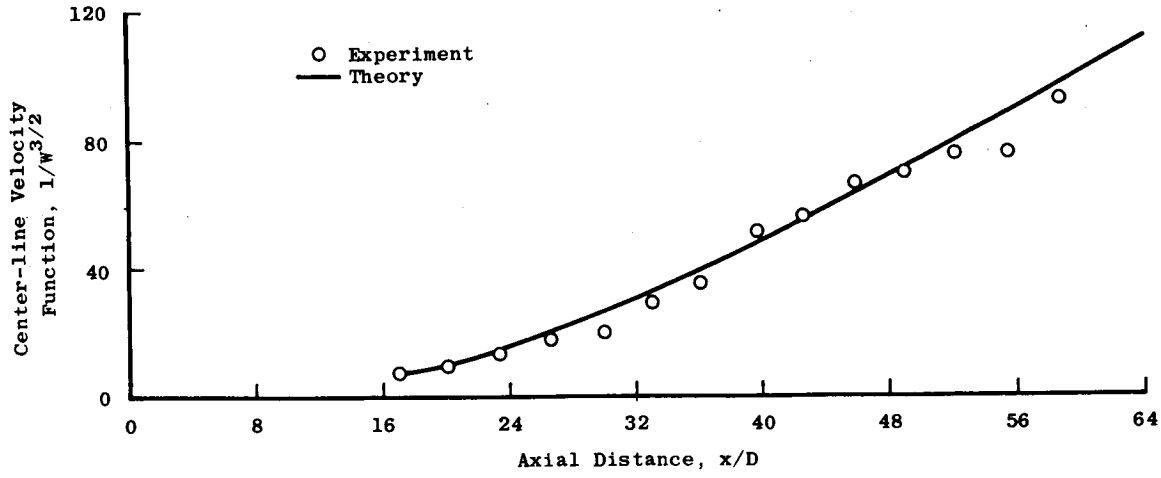

(a) Variation of $1/W^{3/2}$ with x/D.

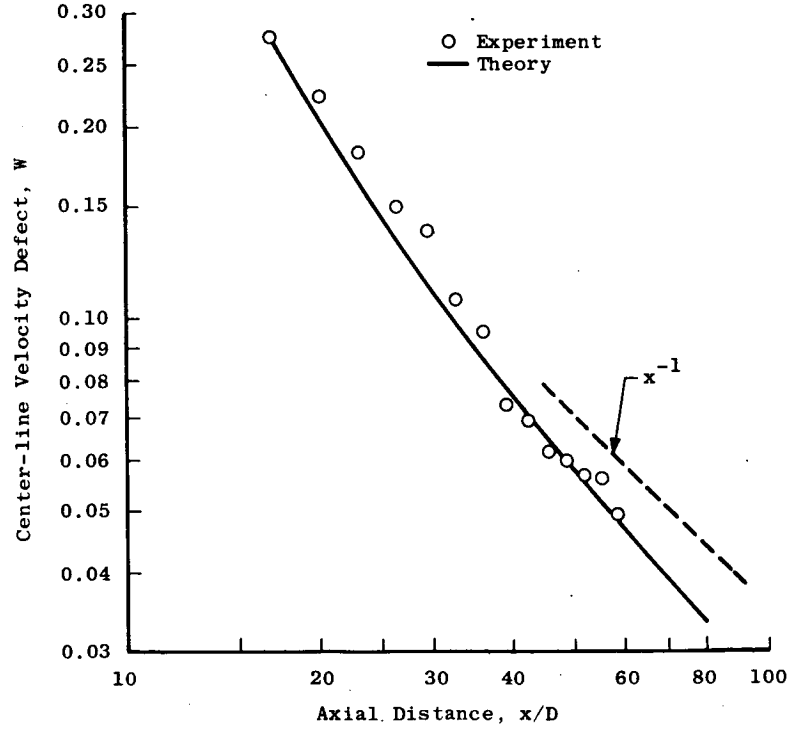

(b) Log plot of W against x/D.

Figure 20.- Test case 17 – Demetriades axisymmetric wake. $M_e = 3$.

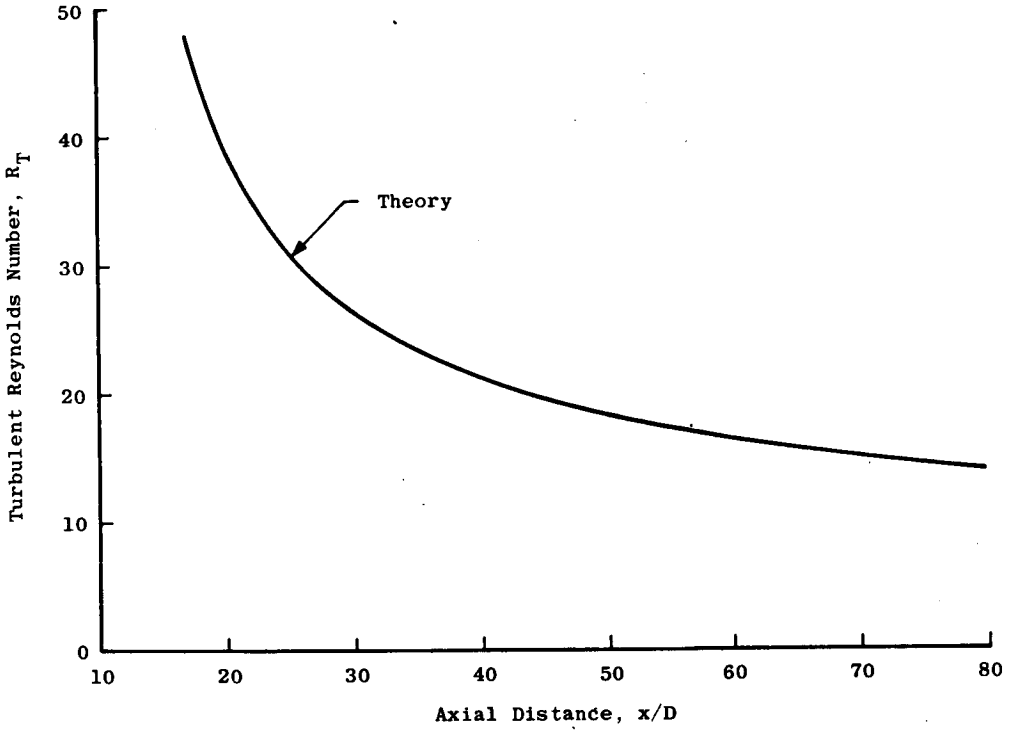

(c) Variation of R_T with x/D.

Figure 20.- Concluded.

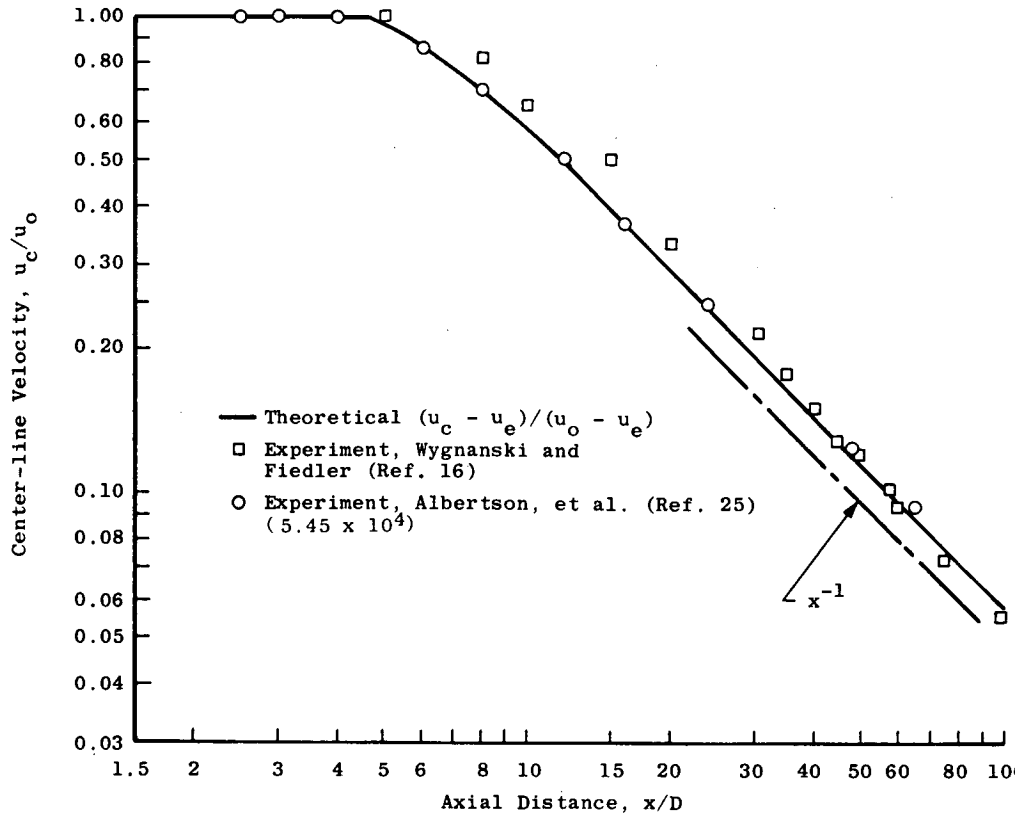

(a) Variation of u_c/u_o with x/D.

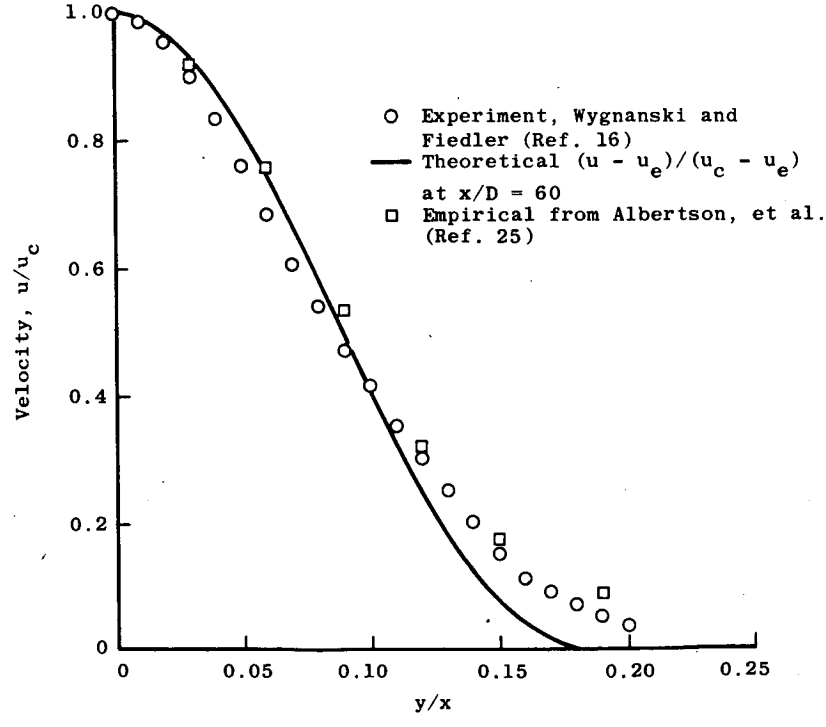

(b) Velocity profile.

Figure 21.- Test case 18 – Fully developed axisymmetric jet into still air.

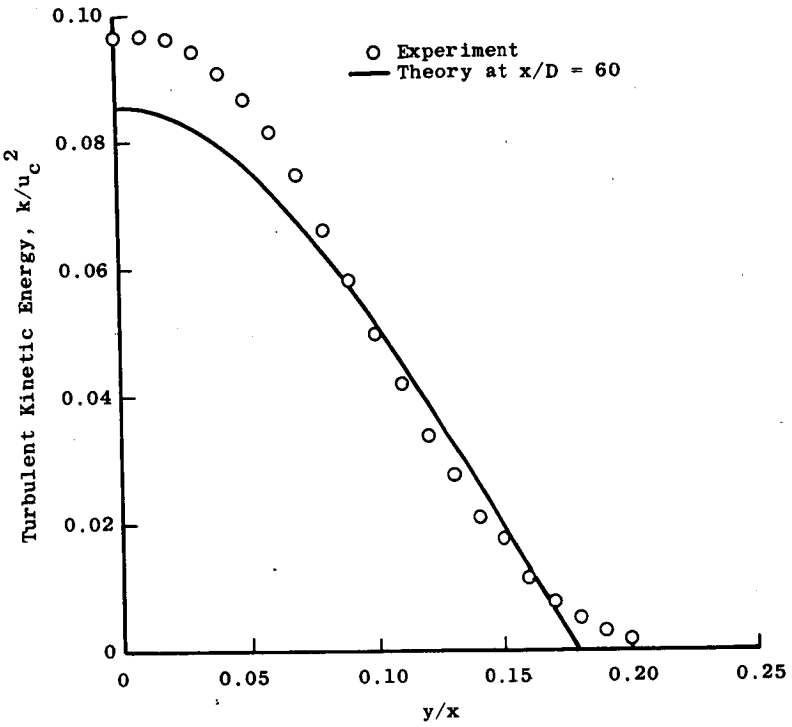

(c) Turbulent kinetic energy profile.

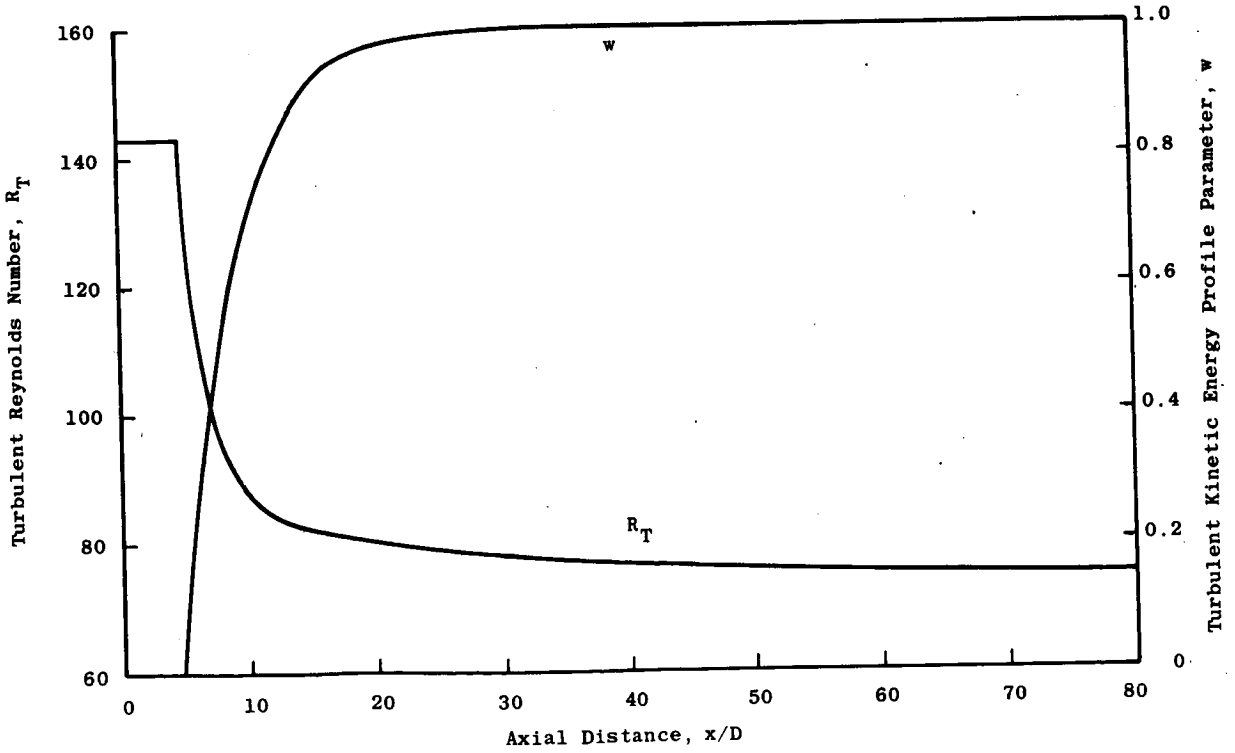

(d) Variation of R_T and w with x/D.

Figure 21.- Concluded.

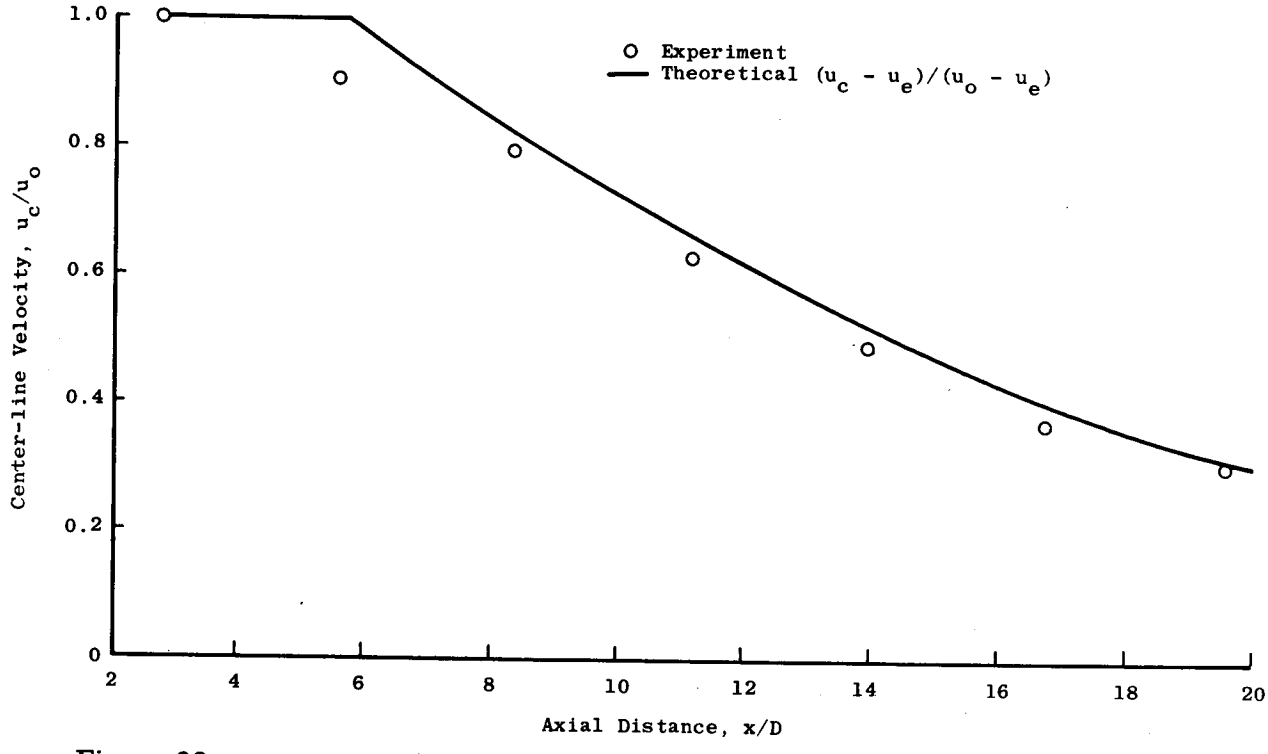

Figure 22.- Test case 19 – Heated axisymmetric jet into still air. $M_o = 1.36$.

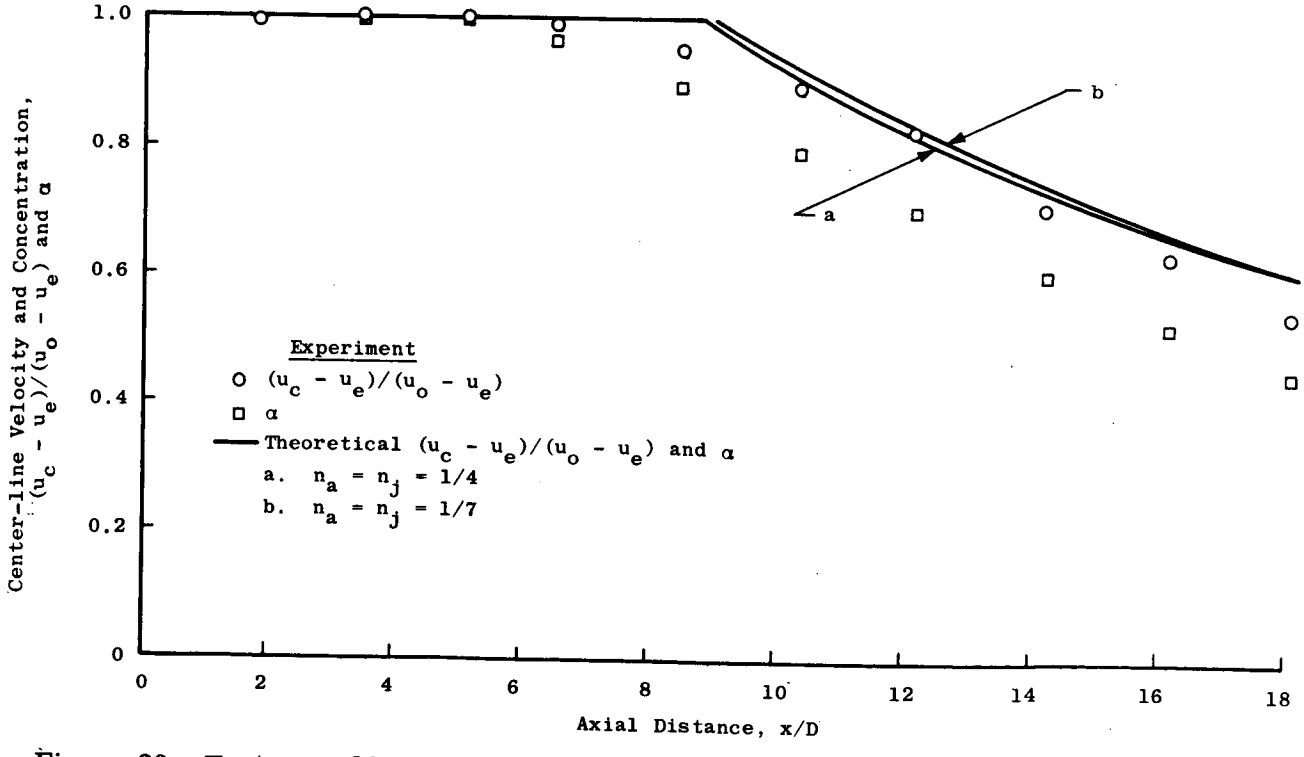

Figure 23.- Test case 20 – Paulk axisymmetric jet in moving stream. $u_e/u_o = 0.48$.

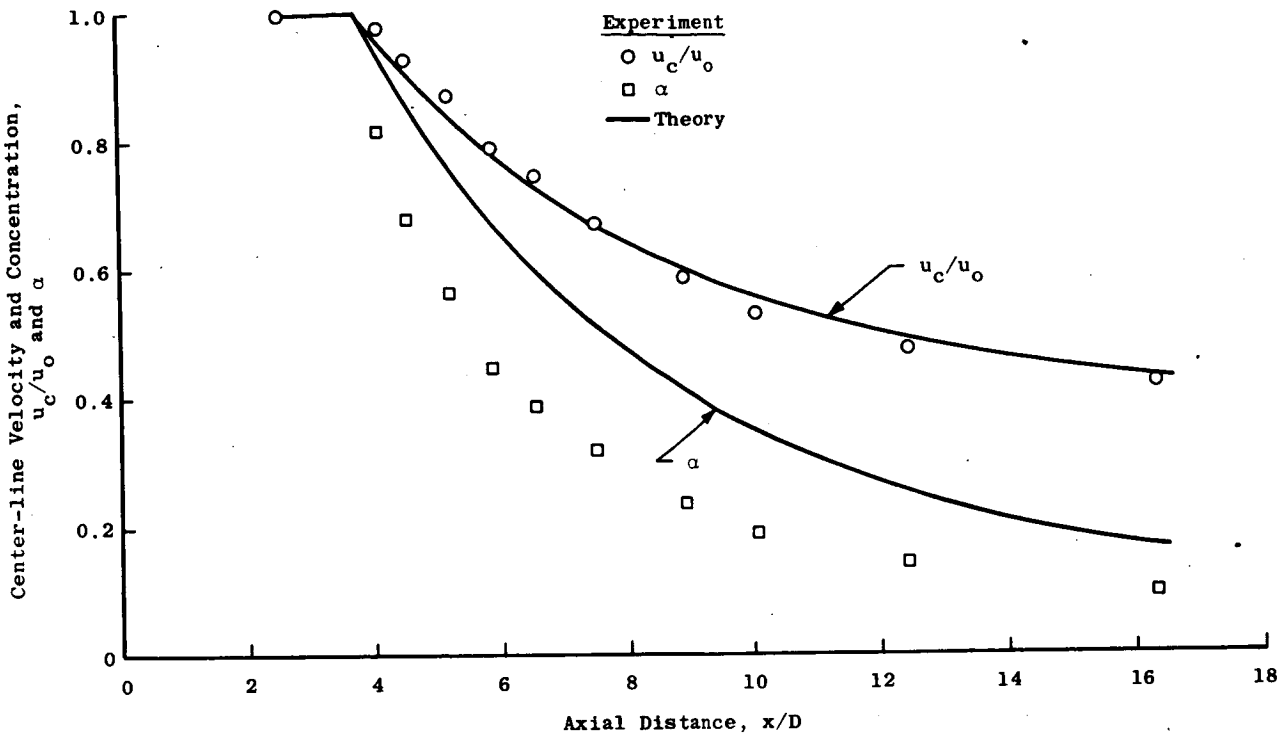

(a) Computations started at x/D = 2.575.

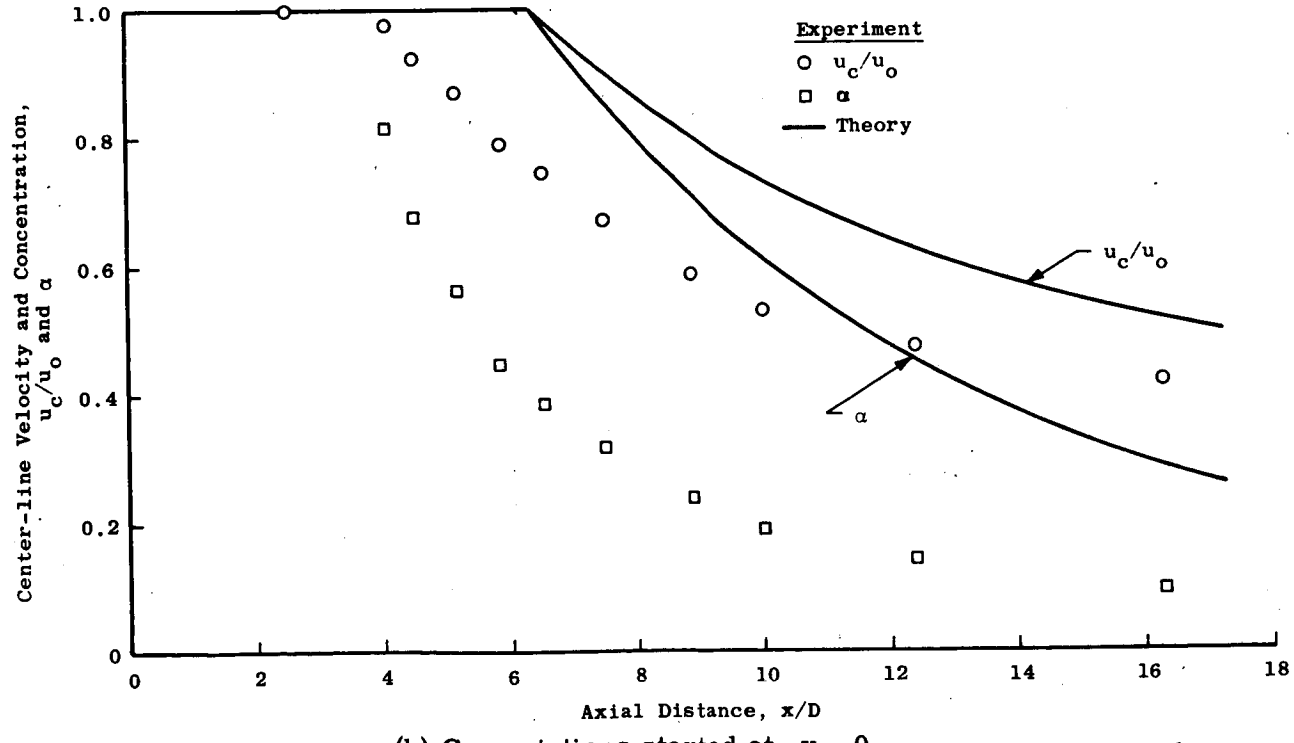

(b) Computations started at x = 0.

Figure 24.- Test case 21 – Chriss H_2 jet in moving stream. $u_e/u_o = 0.31$.

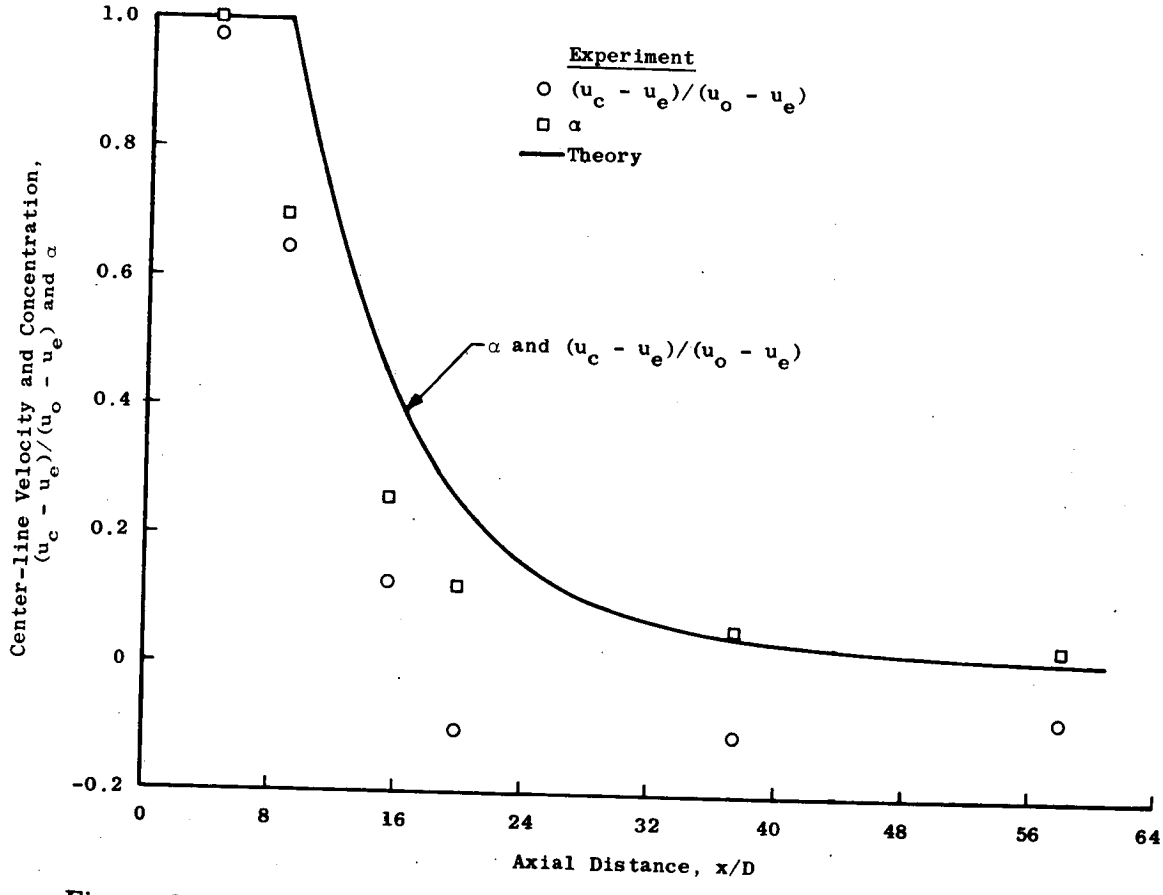

Figure 25.- Test case 22 – Eggers H_2 jet in moving stream. $M_e = 2.5$.

DISCUSSION

S. W. Zelazny: You assume that the Schmidt number was unity in your analysis. Wouldn't it be a simple exercise to remove that restriction by introducing an additional equation?

C.E. Peters: Yes sir, we plan to do that. It's a little frustrating because obviously I have access to Tom Harsha, who sits 15 feet away, and for those flows where I'm interested in a nonfully developed case or nonunity Schmidt number I can always use the finite-difference results. But there are certain flows that I can handle with the integral method we can't handle yet with the finite-difference method. So I will probably go ahead and try to do something to approximately handle nonunity Schmidt number.

S. C. Lee: You mentioned this method you have has some advantage over finite-difference schemes.

C. E. Peters: I didn't refer to it as an advantage, I called it a difference. It's a different set of approximations. Instead of assuming an a_1 function we just assume that the turbulent kinetic energy profile shapes are invariant as a different approach.

S. C. Lee: Perhaps you could summarize for us what would be the difference between this method and the finite-difference method as Harsha presented it.

C. E. Peters: The point is that my kinetic-energy profiles are universal in the given position in terms x/x_{core}. Because of the variable-density and variable-velocity ratio, the shear profile varies from flow to flow; that is, the normalized shape of the shear profile. Therefore, a_1 varies in shape from flow to flow, a condition implied through the whole analysis. I backed it out for some flows, and it does vary from flow to flow. So it's an alternate approximation to saying something about a_1. That's the only fundamental difference. Tom and I are using essentially the same dissipation, and, of course, in return for my specifying the profile shape of kinetic energy, I don't have to say anything about diffusion.

M. V. Morkovin: I think this is another case where we can benefit from the comparisons of different methods. Could you tell us something about your general experience, when you prefer to use Harsha's method to yours and how much more complex it is. I gather you do have some problems in sensitivity to initial conditions. If you could give us a little bit of briefing on that, I think it would be highly valuable.

C. E. Peters: I'll give you my experience first and Tom can comment on it if he likes. The implication of my being able to use a fully developed initial shear stress up to a velocity ratio of 0.25 merely says that these flows are strong shear flows, and they wipe out any small inaccuracies in the initial condition fairly quickly. So that seems to be a viable procedure. When the flows become wake-like in nature, of course, the initial conditions persist indefinitely; in that case my analysis is not applicable at all. For example,

if the hole never fills up, it's not useful. So I limit it to a velocity ratio of maybe 0.7 or 0.8 as the upper limit. I haven't tried to define carefully an upper limit here. Certainly, the finite-difference method is much more powerful in a sense of handling nonsimilar initial conditions and so forth. It's interesting to note the sort of generalized information one can back out with an alternate set of assumptions. For example, about a_1 profiles. So in addition to the practical requirement that we have a better transport model for our "nuts and bolts" engineering calculation schemes, we are also interested in some of the implications in general.

Anon.: Which costs more?

C. E. Peters: This is embarrassing for me because Harsha's program runs faster. But one of the reasons is that this program is a mess; it does lots of different things. This regime is far beyond what we were talking about in this particular calculation. We even do circulating flows with them by using patched up techniques. So the program is not optimized for this kind of flow. If we build a constant-pressure version, I am sure we can get our run time down perhaps an order of magnitude.

I. E. Alber: Your calculation of the spreading parameter variation with Mach number for the two-dimensional shear layer shows quite an increase in the variation of sigma with M. That is your figure 10. Now in this same calculation by Harsha, which I believe is a very similar model to yours, he shows hardly any variation at all.

C. E. Peters: We can't explain that – it's different. Tom, would you care to comment?

P. T. Harsha: Well, the only comment I could make really is that with shear layers I was forced to use an almost patently ridiculous a_1 model which Peters does not have to use because his a_1 comes out of shear stress profile and kinetic energy profiles. I would suspect that the problem is that the a_1 model that I used is simply inappropriate for the shear layer.

J. M. Eggers: I was wondering if you or anyone else here could comment on what we could do to improve the modeling in the transition region to get rid of this somewhat atrocious inflection point at the end of the core region.

C. E. Peters: The sharp corner on the center-line velocity distribution is characteristic of integral methods, at least as we have put them together. It doesn't bother me very much because most of the required information is not centered in that particular region, but the finite difference smooths it out. That's the idea of patching together two regimes discontinuously. It's bound to give a sharp corner with an integral method without some relaxation of profile shapes locally or something.

D. B. Spalding: I have a question and a comment about R_T. The question is a simple one – in the paper R_T seems to be defined twice, once it has the difference between

u_c and u_a on the top and in the second it has the square of those. Which of those was actually used?

C. E. Peters: I think the difference comes because when you plug in the midpoint velocity profile slopes, it is in terms of delta u over width and I think that's where it comes from.

D. B. Spalding: The other remark I want to make is that this quantity appears to be related to the ratio of the production term to the dissipation term which Rodi found also to be significant, and it will be interesting when we have time just to compare whether there was a quantitative connection between your function of R_T and our function of production over dissipation.

C. E. Peters: Yes, I certainly agree. We haven't had time to give much thought as to what this R_T function means in terms of structure, but it would be nice if we could at least rationalize, in terms of energy spectrum or whatever, why the length scale changes or the R_T changes the effective dissipation.

D. B. Spalding: At least you can see that with your definition, when u_c equals u_a, there will be no shear stress, so production is zero. And so R_T is zero; it's the same as $R_{p/\epsilon}$ is equal to zero. Even closer quantitative connections are being worked out.

C. E. Peters: It was also interesting for me to read in Joe Schetz's written version that the constant in his eddy-viscosity model perhaps should be related to a similar parameter to this – the ratio of U prime over delta U. So, this parameter is obviously developed by mean flow correlations during the near field of the wire and jet series, and I just stumbled across it. I think it is better than a mean flow parameter, such as Mach number or some density parameter, and I think it is related to the turbulent structure.

S. Corrsin: I was interested in R_T because the numbers look so much larger than the ones I computed 15 years ago.* Did you compute it for a wake also?

C. E. Peters: Yes, it was shown in the paper I think on the Chevray case. Remember my length scale is the full width of the shear layer; that is, from the centerline out to the outer edge.

S. Corrsin: Well, I was just looking at my paper from 1957 in which is used the half-width and the full-velocity difference. I got a value of 12 for Townsend's wake.

C. E. Peters: I didn't do the two-dimensional wake.

S. Corrsin: And for the round jet, I defined it in terms of the momentum diameter and it came out to be 15.

---

*Corrsin, S.: Some Current Problems in Turbulent Shear Flows. Symposium on Naval Hydrodynamics (Washington, D.C.), Sept. 24-28, 1956, pp. 373-400.

C.E. Peters: My number of 75 for the asymptotic value for the fully developed jet is consistent, considering the difference in length scale definition, with the number tabulated experimentally by B. G. Newman.

S. Corrsin: By whom?

C. E. Peters: Newman, in his survey paper a few years ago. So I think it is consistent with other quoted information.

S. Corrsin: I can make a physical comment about this concept. I first heard it suggested back in the early 1940's by Hans Liepmann, who proposed the idea that perhaps turbulent shear flows tend to keep themselves in a state of lower critical Reynolds number based on the turbulent viscosity, and it's a sort of self-destroying system that always disturbs itself violently. That was sort of the reason that I computed these. For bounded flows, they seem to vary more, but the general idea was that for shear flows without boundaries there are probably universal constants for each geometry.